HHS Public Access

Author manuscript

Acta Biomater. Author manuscript; available in PMC 2017 April 15.

Published in final edited form as:

Acta Biomater. 2016 April 15; 35: 166–184. doi:10.1016/j.actbio.2016.02.017.

Decellularized skin/adipose tissue flap matrix for engineering vascularized composite soft tissue flaps

Qixu Zhang[*], **Joshua A. Johnson**, **Lina W. Dunne**, **Youbai Chen**, **Tejaswi Iyyanki**, **Yewen Wu**, **Edward I. Chang**, **Cynthia D. Branch-Brooks**, **Geoffrey L. Robb**, and **Charles E. Butler**

Department of Plastic Surgery, The University of Texas MD Anderson Cancer Center, Houston, TX 77030, USA

Abstract

Using a perfusion decellularization protocol, we developed a decellularized skin/adipose tissue flap (DSAF) comprising extracellular matrix (ECM) and intact vasculature. Our DSAF had a dominant vascular pedicle, microcirculatory vascularity, and a sensory nerve network and retained three-dimensional (3D) nanofibrous structures well. DSAF, which was composed of collagen and laminin with well-preserved growth factors (e.g., vascular endothelial growth factor, basic fibroblast growth factor), was successfully repopulated with human adipose-derived stem cells (hASCs) and human umbilical vein endothelial cells (HUVECs), which integrated with DSAF and formed 3D aggregates and vessel-like structures *in vitro*. We used microsurgery techniques to re-anastomose the recellularized DSAF into nude rats. *In vivo*, the engineered flap construct underwent neovascularization and constructive remodeling, which was characterized by the predominant infiltration of M2 macrophages and significant adipose tissue formation at 3 months postoperatively. Our results indicate that DSAF co-cultured with hASCs and HUVECs is a promising platform for vascularized soft tissue flap engineering. This platform is not limited by the flap size, as the entire construct can be immediately perfused by the recellularized vascular network following simple re-integration into the host using conventional microsurgical techniques.

Graphical abstract

Schematic representation of *ex vivo* microvascular free dermal/adipose flap engineering. DSAF is prepared from the donor rat and recellularized with the hASCs and HUVECs *in vitro*. Following vascular reanastomosis in the recipient site, the engineered flap construct, which creates a pro-

[*]Corresponding author: Qixu Luke Zhang, MD, PhD, Assistant Professor, Department of Plastic Surgery, The University of Texas MD Anderson Cancer Center, 1515 Holcombe Blvd. Houston, TX 77030, USA, Tel: +1 713-563-7565, Fax: +1 713-563-0231, lukeqixu@yahoo.com.

This work was presented in part at the Society for Biomaterials annual meeting in Boston on April 12, 2013.

All authors have no disclosures related to this work.

Author contributions

Q.Z. conceived and supervised the project, designed experiments, analyzed data, and wrote the paper. Q.Z., J.J., L.D., Y.C., T.I., and Y.W. performed experiments. C.D.B. coordinated the project. E.I.C., G.L.R., and C.E.B. contributed reagents, coordinated the project, and analyzed data.

regenerative environment, could activate an M2 macrophage–mediated constructive remodeling process *in vivo*. With this strategy, DSAF could be translated as a commercial tissue engineering product for personalized tissue repair and regeneration. hASCs: human adipose-derived stem cells; HUVECs: human umbilical vein endothelial cells.

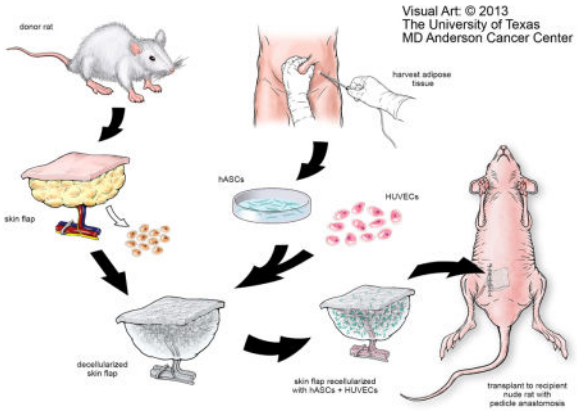

Keywords

vascularized composite tissue flap engineering; soft tissue flap engineering; adipose tissue engineering; skin/adipose tissue flap matrix; extracellular matrix scaffold; decellularization

1. Introduction

Traumatic injury or tumor resection can result in substantial soft tissue loss that requires surgical reconstruction with autologous soft tissue flaps. However, this approach is often limited by a lack of high-quality autologous flaps and by donor site morbidity. One alternative strategy to using autologous tissue flaps is using allogenic tissue flaps. Vascularized composite tissue allotransplantation is a clinical reality in plastic and reconstructive surgery [1]; more than 100 composite tissue allotransplantations have been successfully performed in humans and have included such diverse sites as the hand, abdominal wall, femoral diaphysis and knee, peripheral nerve, larynx, and face [2, 3]. Unfortunately, the survival of composite tissue allotransplantation without rejection depends on the use of chronic nonspecific and novel specific immunosuppressive medications, many of which carry a risk for neoplasms, opportunistic infections, and/or end-organ toxicity [4].

Engineered composite tissue flaps, which do not require the use of immunosuppression, may offer an ideal, clinically viable alternative to both autologous flaps and allogenic tissue flaps. Recently, tissue engineers have reached several milestones in the regeneration of organs including the heart, lung, and liver using decellularized whole-organ matrix scaffolds [5–7]. The native platform, especially its vascular network within the organ extracellular matrix (ECM), has an important role in vascularized organ engineering. A similar concept has been applied in vascularized composite tissue engineering. In one study, researchers decellularized a segment of porcine small bowel with its artery and vein structure and repopulated it with multiple types of cells *in vitro* [8]. Another study showed that with blood perfusion, this kind of bioartificial vascularized scaffold, which had been recellularized with

porcine bladder smooth muscle cells and urothelial cells and endothelial progenitor cells, remained intact for 1–3 hours in a porcine model [9]. Furthermore, a similar bioartificial vascularized scaffold, which had been recellularized with a patient's autologous muscle cells and fibroblasts and endothelial cells and implanted into a patient's arm, had patent vessels with functional circulation and tissue viability 1 week postoperatively [10]. On the basis of these promising results, which indicated the feasibility of bioengineering a human tissue with innate vascularization, Aubin et al. decellularized the native cardiac muscle of a rat to establish a coronary artery tissue flap; its re-endothelialization *in vitro* indicated that it had great potential for further application [11]. More recently, Jank et al. created decellularized limb composite tissue matrix. The recellularized limb tissue matrix–multiple cells construct showed perfusion in a re-endothelialized vascular conduit in a short-term non-survival procedure in a rat model [12]. Overall, the use of decellularized composite tissue matrix to engineer vascularized composite tissue has progressed much in recent years. However, unlike the closed system of the whole-organ matrix, the open system of the composite tissue flap matrix poses many challenges, and most models are still in need of long-term observation *in vivo*.

Skin/adipose tissue flaps are the workhorses of routine reconstructive microsurgery. Thus, skin/adipose tissue flap engineering has tremendous impact in the field of reconstructive surgery. Studies have shown that a completely decellularized skin flap matrix retains its vascular structure intact [13, 14]. However, details about the characterization of the acellular skin flap matrix are lacking, and the interaction between the cells and scaffold matrix during the remodeling process has not yet been investigated *in vitro* or *in vivo*.

As one of the biggest reconstructive microsurgery centers in the world, we have performed more than 3,200 free flap transfers in the last 5 years (unpublished data). Our experience indicates a need for engineering composite tissue flaps to repair large tissue defects to ultimately avoid donor site injury and morbidity. Thus, the purpose of the present study was to establish a platform for using a decellularization approach to engineer soft tissue free flaps that have more flexible clinical applicability. We used a perfusion decellularization protocol to process skin/adipose tissue flaps from rats. The decellularized skin/adipose tissue flap (DSAF) was comprehensively characterized with respect to its three-dimensional (3D) architecture, biomolecular patterning, and bioactivity. The biocompatibility of DSAF was tested by integrating it with human adipose-derived stem cells (hASCs) and human umbilical vein endothelial cells (HUVECs). Prevascularized and recellularized DSAF with a dominant vascular pedicle and integrating multiple cell types was then implanted into a rodent model using conventional microsurgical techniques, and the *in vivo* response, biocompatibility, and remodeling properties of DSAF were evaluated. The findings of the present study may inform the development of a platform for designing and fabricating 3D vascularized dermal/adipose tissue constructs that can be used to repair extensive soft tissue defects.

2. Materials and methods

2.1. Creation of the DSAF bioscaffold

All animal handling and experimental procedures strictly followed the research protocol approved by MD Anderson's Institutional Animal Care and Use Committee and the National Institutes of Health guidelines for animal welfare. Groin skin/adipose tissue flaps (2×4 cm^2) were harvested from euthanized 8- to 10-week-old male Fischer 344 rats (Harlan Laboratories, Indianapolis, IN). The flap pedicle included the superficial epigastric artery and vein plus segments of the femoral artery and vein and the femoral nerve. Immediately after harvest, the femoral artery was catheterized with a 24G catheter (BD Biosciences, San Jose, CA), and the flap was irrigated with normal saline through the femoral artery until only clear normal saline flowed from the femoral vein. The flaps were frozen at −80°C and thawed at room temperature for 3 cycles and were then processed with chemical detergents as described previously [15]. For each flap, the artery was catheterized, and the flap was connected via the catheter to a Masterflex pump perfusion system (Cole-Parmer, Vernon Hills, IL) and perfused with ultrapure water (2 ml/min) for 1 day at room temperature. The flap was then treated with 0.5 M NaCl for 4 hours, 1 M NaCl for 4 hours, and ultrapure water overnight; this saltwater perfusion procedure was repeated once. After treatment with 0.25% trypsin/ethylenediaminetetraacetic acid for 2 hours at 37°C and washing with deionized water for 1 hour, the flaps were processed with isopropanol overnight with agitation. The flaps were then treated with 1% Triton X-100 for 2 days (1 change daily), washed in ultrapure water for 2 days (3 changes daily), and rinsed in phosphate-buffered saline (PBS) for 1 day within the perfusion system. DSAF was sterilized using 70% ethanol and rinsed in PBS. DSAF was stored at 4°C in PBS containing 1% penicillin/streptomycin until use (Fig. 1A–D).

2.2. Characterization of DSAF

2.2.1. Histological and immunohistochemical analysis—Native skin/adipose tissue (NSAF) and DSAF (n=3, respectively) were fixed in 10% formalin, embedded in paraffin, and sliced into 5-μm sections. Slides of the paraffin-embedded samples were processed for histological and immunohistochemical (IHC) staining. The slides were stained with hematoxylin and eosin (H&E), Masson's trichrome, and 4′,6-diamidino-2-phenylindole (DAPI). The slides were also stained using antibodies against vascular endothelial growth factor (VEGF) and basic fibroblast growth factor (bFGF; both from Oncogene Science, Cambridge, MA) and antibodies against major histocompatibility complex antigen class I (MHC-I) and laminin (both from Abcam, Cambridge, MA). For IHC staining, the slides were placed in antigen retrieval citrate buffer (Biogenex, Fremont, CA) in a 95°C steamer for 10 minutes. Endogenous peroxidases were blocked with a peroxide block (Innogenex, San Ramon, CA), and nonspecific binding was blocked with normal goat serum (Vector Laboratories, Burlingame, CA). Sections were incubated with the primary antibodies at 4°C overnight. After the slides were washed, they were subjected to the application of a biotinylated secondary antibody for 30 minutes, treatment with a streptavidin-horseradish peroxidase complex (Vectastain ABC kit, Vector Laboratories) and diaminobenzidine solution (DAB kit, Vector Laboratories), and counterstaining with hematoxylin. After

staining, the slides were dehydrated and mounted and then imaged using an Olympus IX71 microscope (Olympus, Center Valley, PA).

2.2.2. DNA assessment and quantification—Cell removal was quantified by measuring the nucleic acid concentration with the Quant-iT PicoGreen dsDNA assay kit (Molecular Probes) as described previously [16]. Briefly, native tissues and decellularized samples (n=3, respectively) were digested in 1 mg/ml papain (Sigma, St. Louis, MO) at 60°C for 48 hours. The samples were then centrifuged at 12,000 rpm at 4°C for 10–15 minutes. Supernatants from the samples were measured for fluorescence intensity using a VersaFluor spectrofluorometer (BioRad Laboratory Inc., Hercules, CA), and the measured DNA quantity was normalized to the initial dry weight of the tissue.

2.2.3. Sulfated glycosaminoglycan content—The sulfated glycosaminoglycan (GAG) contents of native tissues and decellularized samples were quantified using an Alcian blue colorimetric assay kit (sGAG Dye Binding Assay, ALPCO, Salem, NH) as described previously [16]. Briefly, the samples (n=3 in each group) were lyophilized, digested with papain, and then incubated with Alcian blue dye. Absorbance of the samples at 600–620 nm was measured with a DU730 UV/Vis spectrophotometer using chondroitin sulfate (Sigma) as the standard. The GAG content was normalized to the initial dry weight of the samples.

2.2.4. Scanning electron microscopy—DSAF samples (n=3) were frozen at −80°C and dried through lyophilization. The dry samples were coated with a 25-nm layer of a platinum alloy under vacuum using a Balzer MED 010 evaporator (Technotrade International, Manchester, NH) and immediately flash-carbon-coated under vacuum. The samples were examined with a JSM-5910 scanning electron microscope (JEOL, Peabody, MA) at an accelerating voltage of 5 kV. Fiber size was measured using the ImageJ software program (National Institutes of Health, Bethesda, MD).

2.2.5. Porosity measurement—The porosity values of the DSAF samples (n=3) were measured by liquid displacement as described previously [17]. Ethanol was used because it penetrates easily into pores and does not induce shrinkage or swelling.

2.2.6. Vascular structure measurement—The microcirculatory network of DSAF was revealed by injecting 1 ml of mixed Microfil-117 (Flow Tech, South Windsor, CT) solution into the artery pedicle at a rate of 1 ml/min. DSAF was stored at 4°C overnight and then imaged using a Discovery V8 microscope (Zeiss, Oberkochen, Germany).

2.3. Recellularization of DSAF

2.3.1. hASC and HUVEC culture—All procedures involving human tissue samples were approved by MD Anderson's Institutional Review Board and conducted in accordance with MD Anderson's research guidelines. Samples of subcutaneous adipose tissues resected from the abdominal wall area in patients undergoing reconstructive surgery were collected. (These tissues are usually discarded after surgery.) hASCs were cultured using our established protocol [15]. hASCs were confirmed by adult stem cell differentiation assays (GIBCO stem cell differentiation kit, Life Technologies). Adipogenesis of hASCs was assessed by Oil Red

O staining. Osteogenesis was assessed by Alizarin Red S staining. Chondrogenesis was assessed by collagen type II staining as described in section 2.2.1. Commercially available HUVECs (Lonza, Walkersville, MD) were cultured in endothelial in growth medium supplemented with bovine brain extract according to the manufacturer's instructions. Cells were maintained in 25 cm^2 flasks until they were plated onto glass slides or DSAF scaffolds. The medium was replaced every other day, and the cultures were maintained in a humidified 5% CO_2 incubator at 37°C.

2.3.2. Seeding HUVECs and hASCs on DSAF—hASCs or HUVECs within three passages were harvested and plated onto glass slides or DSAF scaffolds at a density of 2.5×10^4 cells/cm^2 and then stained with Calcein AM and Ethidium homodimer-1 (EthD-1) using the LIVE/DEAD Viability/Cytotoxicity Kit (Molecular Probes) according to the manufacturer's instructions. Samples (n=3 in each group) were examined with an Olympus IX81 confocal fluorescence microscope on days 1 and 7 after cell seeding. For the hASC/HUVEC coculture, 2×10^5 HUVECs in 200 μl of medium were injected into the artery and vein pedicle, respectively, and an additional cell mixture of 1×10^6 hASCs and 2×10^5 HUVECs suspended in 1 ml of growth medium was injected into the DSAF scaffold at 10 sites (3 on the dermis side and 7 on the fat pad side). DSAF was statically cultured for 7 days. The cell-seeded DSAF was stained with a mouse polyclonal antibody against CD31 (1:300; Abcam) and then with fluorescein isothiocyanate goat anti-mouse immunoglobulin G (heavy and light chains; 1:500). All cells were stained with DAPI. Three samples were prepared under each condition at each time point. Samples were imaged with an Olympus IX81 confocal fluorescence microscope. Cell morphologic features (perimeter, area, and roundness) were measured using Photoshop CS 5.1 image-processing software (Adobe, San Jose, CA). Roundness was defined as $4*\pi*\text{area}/(\text{perimeter})^2$.

2.4. Transfer of the DSAF-cells construct as a free flap

All animal procedures were approved by MD Anderson's Institutional Animal Care and Use Committee and met all requirements of the U.S. Animal Welfare Act. Eight- to ten-week-old syngeneic athymic female nude rats (National Institutes of Health) were used to minimize cellular and humoral immunological responses to human cells. The rats were randomly divided into three groups: group A received cell-seeded DSAF implanted with microsurgery; group B received cell-seeded DSAF implanted without microsurgery; and group C received DSAF alone implanted without microsurgery. Anesthesia in rats was induced and maintained with isoflurane in oxygen (0.5–2%, 3–5 L/min). For the group B and C rats, a 2-cm incision was made in the groin area, the engineered cell-seeded DSAF or DSAF alone was carefully implanted subcutaneously, the skin incision was closed with a 4/0 Prolene suture, and the constructs were left in place for 3 months (n=5 for both groups), after which time the animals were humanely killed and the constructs explanted. For the group A rats, groin dissection was performed to isolate the deep femoral artery-vein pedicles; nerves were preserved to avoid interfering with the animals' movement. The vascular pedicle of the cell-seeded DSAF was anastomosed with the recipient femoral artery and vein with a 10/0 Nylon suture under a Medlink 2880 surgical microscope (Montrose, MN). The nerve structure was joined with the recipient femoral nerve in an end-to-side fashion. After vascular perfusion was confirmed, the skin incision was closed, and constructs were left in place for 7 days

(n=4) or 3 months (n=5), after which time the animals were humanely killed and the constructs explanted. The constructs from all three groups were subsequently dissected, cross-sectioned, and fixed in 10% formalin and embedded in paraffin for histologic analysis. The samples were stained with H&E and Masson trichrome and with antibodies against HuNu (for human cell nuclei, 1:200, Millipore, Bedford, MA), antibodies against CD31, smooth muscle actin (SMA), and CD68 (all at 1:200; Abcam), and antibodies against CD163 and CD80 (both at 1:200; AbD Serotec, Raleigh, NC) as described in section 2.2.1. The slides were imaged using the Vectra multispectral slide analysis system (PerkinElmer, Waltham, MA). The resulting multispectral images were analyzed using Photoshop CS 5.1 image-processing software. The following quantities in each slide were measured: total area of the sample, total area of the adipose tissue, and total area of remodeled tissue. These data were used to calculate the percentage of the total area that was adipose tissue and the percentage of the total area that was remodeled in individual groups. Positive cell staining was quantified visually using random fields over the entire construct.

2.5. Statistical analysis

Data were presented as means ± standard deviations. Data were analyzed using one-way analysis of variance and the Student t-test with the SigmaStat software program (version 3.5, SyStat, USA). *P* values of less than 0.05 were considered significant.

3. Results

3.1. Characterization of DSAF

Microfil was easily injected into the flap matrix through the artery pedicle. Microfil images revealed that the femoral artery and its branch, the superficial inferior epigastric artery, remained intact after decellularization. The microcirculatory network was well preserved in the decellularized fat pad, and the number of perforators ascending to the acellular dermis suggested that the subdermal blood plexus was well retained (Fig. 1E–G).

H&E and DAPI staining revealed that cell nuclei were present in native tissues but absent in DSAF (Fig. 2A–D). The DNA content was significantly reduced from 0.38 μg/mg DNA/dry weight in the native skin to 0.04 μg/mg DNA/dry weight in the decellularized dermis ($P<0.05$) and from 0.35 μg/mg DNA/dry weight in the native fat pad to 0.05 μg/mg DNA/dry weight in the decellularized fat pad ($P<0.05$). These results indicated that a significant amount of cellular components had been removed in the DSAF samples. H&E staining also showed that oil components were completely removed, while blood vessels and nerves structures were well retained in DSAF (Fig. 2A).

Masson trichrome staining showed that collagen was a major component of native adipose tissue and that the collagen component was maintained in DSAF after decellularization (Fig. 2C). Staining with Alcian blue revealed that GAG was also retained in DSAF (1.56±0.42 μg/mg GAG/dry weight in the decellularized dermis; 0.54±0.58 μg/mg GAG/dry weight in the decellularized fat pad). IHC analysis indicated that laminin was distributed in the vessels, nerves, and nanofibrous structures in DSAF (Fig. 2E). bFGF and VEGF, which play important roles in angiogenesis and neovascularization, were also retained in DSAF. In native adipose tissue, both growth factors were found mainly at blood vessels and

surrounding adipose cells and gland cells. After decellularization, the growth factors were found along vessels, nerves, and nanofibrous structures (Fig. 2F, G). IHC analysis also revealed that MHC-I was located mainly at the blood vessels in native adipose tissue. The absence of MHC-I in DSAF indicated the removal of alloantigenicity from DSAF (Fig. 2H).

Scanning electron microscopy (SEM) images confirmed that cells were absent in DSAF, leaving 3D porous structures in the fat pad (porosity = 83.6 ±7.8%; Fig. 2I). Nanofibrous structures of ECM were well maintained in DSAF (fiber size = 302.3 ±90.4 nm; Fig. 2I). The decellularized femoral artery remained elastic and patent (Fig. 2J).

3.2. Recellularization of DSAF

3.2.1. hASC integration with DSAF—Live/dead cell staining with Calcein AM and EthD-1 indicated that DSAF supported hASC survival and proliferation (Fig. 3). After plating, the hASCs attached well to DSAF and proliferated from day 1 through day 7. Quantitative analysis of cell morphologic features revealed significant differences between cells cultured on DSAF and cells cultured on 2-dimensional glass slides (Table 1). For example, the hASCs on DSAF were rounder than those on the glass slides and exhibited smaller spreading areas and perimeters ($P<0.05$ for each).

3.2.2. Prevascularization of DSAF—Live/dead cell staining also showed that DSAF supported HUVEC survival and proliferation. When HUVECs were cocultured with hASCs on DSAF scaffolds, more capillary-like structures formed, and they developed an interconnected network of branches by day 7. The vascular pedicle was re-endothelialized by culturing it with HUVECs. Cells cultured on DSAF also formed 3D cellular aggregates *in vitro* (Fig. 3 and Supplementary Videos 1–2).

3.3. Evaluation of the DSAF-cells construct in vivo

Following the removal of the clamps from the anastomosed vascular pedicle, blood immediately perfused the whole DSAF-cells construct. That the construct remained warm and pink without congestion for up to 30 minutes suggested that the functional circulation maintained balanced blood flow (Fig. 4A–C). All animals survived until sample explantation. On day 7, the explant was encapsulated in swollen tissue. When Mircofil-117 was injected through the contralateral femoral artery, it easily went through the vascular pedicle of the engineered flap construct. Using microscopy, we found that the Microfil filled the vessels that grew in the pedicle area instead of the main artery. This suggested that the bypass arteries were perfusing the construct and that the main artery was not functional at this time (Fig. 4D). Unlike the constructs explanted at 7 days, the constructs explanted at 3 months were very soft and had a yellow-gold adipose tissue appearance, and the numerous visible blood vessels penetrating the regenerated soft tissue confirmed that it was highly vascularized (Fig. 4D).

Histologic analysis revealed an inflammation reaction, characterized by cellular and vascular infiltration in the tissue at day 7 (Fig. 5A). Unlike the constructs explanted at 7 days, the constructs explanted at 3 months underwent constructive remodeling. Most of the dermis tissue was degraded and remodeled as adipose-fascia tissue, and the remaining small portion

of dense collagen was being remodeled. Compared with its dermis side, the flap construct's fat pad side was fully remodeled, showing mature adipose-fascia tissue formed by adipocytes and few fibroblasts (Fig. 5B, C). The mean percentage of adipose soft tissue at 3 months (78.5±6.8%) was significantly higher than that at 7 days (3.3±1.3%; $P<0.05$) (Fig. 5E). The presence of seeded cells was evaluated by immunohistochemical staining. In the engineered soft tissue, the "donor" cells (i.e., the original HuNu-positive cells) were distinguishable and persistent at 7 days; by 3 months, however, the signal for these cells was fading (Fig. 5D, F). Cells in the vascular and adipose structures stained positively for HuNu, indicating that seeded cells contributed to angiogenesis and adipose tissue development. The peripheral nerve structure showed cellular infiltration at day 7; it was completely repopulated at 3 months (Fig. 5A–C). Abundant CD31- and SMA-positive blood vessels were distributed throughout the capsule, dermis, and fat pad of the explant at 7 days. Accordingly, the pedicle had many intravascular red blood cells (Fig. 6A). Although the main artery pedicle showed myointimal hyperplasia, the soft tissue formation was highly vascularized by numerous CD31- and SMA-positive vessels throughout the explant at 3 months; meanwhile, lots of red blood cells filled the functional vessels (Fig. 6B). As predominant inflammatory cells, many CD68-positive macrophages infiltrated the construct at 7 days. Among these cells, both CD80-positive macrophages (M1 macrophages) and CD163-positive macrophages (M2 macrophages) were found throughout the sample tissue (Fig. 7A). There were significantly fewer M1 macrophages at 3 months than at 7 days ($P<0.05$); most macrophages at 3 months were M2 macrophages. The M2 macrophage–predominant infiltration in the dermis side suggested ongoing constructive remodeling in that area. Much fewer macrophages were present in the fat pad side, indicating that the area was fully remodeled (Fig. 7B–D). Unlike those of group A, the explanted samples of groups B and C were relatively hard, with lots of undegraded dermis; histologic analysis revealed that compared with the group A samples, the group B and C samples showed much more fibrotic remodeling, with lower vascularization and less adipose tissue regeneration, at 3 months (Fig. 8).

4. Discussion

Although decellularized adipose matrix holds tremendous potential for adipose tissue regeneration, recent attempts to engineer adipose tissue have involved only decellularized adipose tissue matrix without the appropriate circulatory network [15, 18, 19]. Consequently, the engineered constructs require lengthy periods to achieve neovascularization and integration with the host tissue. This extra time requirement limits the success of using decellularized matrix in the large-scale regeneration of adipose tissue. Given its unique circulatory system, recellularized and re-endothelialized DSAF can receive immediate blood perfusion, which in large-scale stem cell–bioscaffold constructs would reduce the ischemia duration, thus increasing their function and survival for better constructive outcomes. The present study confirmed the feasibility of this approach. Our data showed for the first time that DSAF—a composite soft-tissue flap matrix recellularized with multiple cell types—can become vascularized 7 days after reanastomosis in the recipient site and achieve fully constructive remodeling with highly vascularized adipose tissue regeneration within 3 months.

In the present study, we applied a perfusion protocol combined with agitation to create the DSAF matrix. We found that this protocol efficiently removed cellular and oil components from the skin and adipose tissues. DSAF had only a little nuclear debris, which may have been due to a small amount of cell nuclear material that remained attached to the DSAF scaffold after decellularization. (Even though implant failure due to a small amount of small-molecular-weight DNA is unlikely, ways to completely remove DNA from DSAF should be identified to achieve 100% safety.) After DSAF decellularization, the native ECM structure was well maintained, and the resultant 3D ECM architecture presented microporous and nanofibrous hybrid structures. The remaining scaffolds were composed mainly of collagen, GAG, and laminin, particularly in the dermis side of DSAF. bFGF and VEGF were mainly located in the fat pad side, indicating a pre-angiogenic property, and the overall absence of MHC-I indicated that the DSAF matrix would be safe from rejection at implantation. IHC analysis showed that the peripheral nerve and vessel structures remained intact in DSAF. Microfil-117 angiography confirmed that DSAF maintained a dominant vascular pedicle and a microcirculatory network that was closely accompanied by peripheral nerve ECM structures. These results indicate that the native 3D structural and biochemical properties of skin and adipose tissue ECM were well-maintained in DSAF and provided molecular and topographical cues for cell seeding and tissue engineering.

Mesenchymal stem cell–based treatments, specifically those used in combination with ECM-based scaffolds for tissue engineering, have expanded substantially in recent years. Not surprisingly, owing to their adult stem cell characteristics and easy isolation with conventional liposuction procedures, which avoid tissue damage better than bone marrow aspiration does, hASCs have been the predominant cell source for adipose tissue engineering [20]. In this study, live-cell staining with Calcein AM proved that hASCs successfully integrated with DSAF *in vitro*. In addition, hASCs on DSAF exhibited *in vivo*–like morphologic features, including smaller areas and rounder shapes. These features, which were significantly different from those of hASCs in 2-dimensional cultures, were likely due to the unique topography cues of DSAF: the DSAF scaffolds had porous nanofibrous structures, which have been reported to affect cellular morphology and function [19, 21–23]. Others have reported that seeded hASCs stabilized HUVECs *in vitro* and that the paracrine activity of hASCs facilitated tissue angiogenesis *in vivo* [24]. For this reason, we applied co-cultured hASCs and HUVECs to re-endothelialize DSAF in the present study. As a result, HUVECs adhered to and proliferated in DSAF and re-endothelialized the vascular pedicle, and vessel branch–like structures grew in DSAF after *in vitro* cell culture. This interaction among hASCs, HUVECs, and DSAF supports the idea that DSAF, with its native ECM properties, provides a suitable niche for effective precellularization and prevascularization.

The host’s immunological responses to implanted cell-biomaterial constructs play major roles in determining the clinical efficacy of the biomaterials used [25]. Macrophages are particularly important immune cells involved in the host’s reaction to the implants [26]. Studies have shown that a muscle or dermal ECM scaffold can promote anti-inflammatory and immunosuppressive responses and activate the M2 macrophage phenotype to support constructive remodeling *in vivo* [27–29]. Although the exact mechanism by which ECM scaffold regulates macrophage polarization is not fully understood, a number of factors have been recognized. For example, certain surface peptides and ligands on the scaffold that have

been exposed by the decellularization process may modulate the immune response [28, 30–32], and the ECM degradation products may have immunomodulatory activity [26]. hASCs, owing to their unique immunomodulatory properties, can also induce the M2 macrophage phenotype [33, 34]. One recent study suggested that 3D topography plays a key role in regulating mesenchymal stem cells' immunomodulatory effects, which can push macrophages towards an anti-inflammatory phenotype [35]. In the present study, the DSAF-cells construct did elicit a foreign-body response in the form of CD68-positive macrophage infiltration. Both M1 and M2 macrophages, which are markers of acute inflammation, infiltrated the implants by day 7; however, there was a trend of the macrophages switching from M1 to M2 status in the following remodeling stage. Unlike the macrophages involved in a severe foreign-body reaction, which results in structural weakening or rapid degradation with severe fibrosis [36], the macrophages present within the implants at 3 months in the present study were almost at a reconstructive remodeling stage (CD163-positive M2 macrophages) and not in an inflammation stage (CD80-positive M1 macrophages). Consistent with the cellular action, IHC staining indicated that mature adipose tissue regeneration occurred in the engineered DSAF. The center portion of the dermis was still in a constructive remodeling stage, with M2 macrophages predominantly distributed, whereas abundant adipocytes in the fat pad side and the area between the fat pad and dermis indicated that these areas were fully remodeled. During construct remodeling, the number of hASCs decreased while the number of host cells increased, suggesting that seeded hASCs play an important role in adipogenesis early on, whereas host cells, probably bone marrow–derived adipocyte precursors, greatly contribute to adipogenesis later on. These results were consistent with those of previous reports [15, 37]. hASCs contributed to adipose regeneration through direct differentiation and/or paracrine action. As others have posited [27–29, 33–35], we believe that hASCs and DSAF worked synergistically to activate M2 polarization and provide a pro-regenerative environment for adipose tissue formation in our model. Hence, our data suggest that the hASCs-DSAF 3D scaffold holds great promise in soft tissue engineering because each component not only directly participates in adipose tissue regeneration but also modulates the host immune response to the engineered constructs.

Vascularization and blood supply are critical to the successful grafting of cell-biomaterial constructs, and researchers have proposed many strategies and techniques to improve neovascularization within implanted bioscaffolds. One strategy is to functionalize scaffolds by introducing biochemical molecules, such as VEGF, to promote vessel formation [38]. Physical components such as nanofibrous structures also have been incorporated into scaffold design to induce neovascularization for tissue engineering [39]. Another strategy for increasing neovascularization involves cell-based treatment with ASCs or ASCs co-cultured with endothelial cells [40]. These strategies are all incorporated into the creation of DSAF, which provides a 3D bioscaffold, contains bFGF and VEGF, and supports hASCs' adhesion and proliferation, making it an ideal platform for co-culturing hASCs and HUVECs for engineering pre-vascularized soft tissue free flaps.

Successful tissue engineering depends on the successful, efficient integration of all components, which allows adequate cellular implantation onto a biomimetic scaffold that will sustain a sufficient cellular mass that can be perfused with a vascular network that can

be integrated with the host circulatory system. As with other decellularized composite tissue flaps, such as small bowel flaps [9, 10], DSAF, with its native dominant vascular pedicle, can be integrated into the host using conventional microsurgical techniques; thus, the size of the engineered construct does not limit is ability to obtain adequate blood supply. In the present study, DSAF was easily incorporated *in vivo*; after anastomosis to the recipient vessels, the recellularized vascular network immediately perfused the native microcirculatory network of DSAF. This type of early blood perfusion delivers oxygen and nutrition to the large-scale biomaterials-cells construct, facilitating its survival, and simultaneously recruits host bone marrow–derived immune cells and progenitor cells for flap angiogenesis, vasculogenesis [41], and tissue remodeling and regeneration. Although the main vascular pedicle was not functional at day 7, the Microfil still went through the bypass arteries in the pedicle area. IHC staining confirmed that a number of large vessels around the pedicle area contained red blood cells and that numerous vascular infiltrations were present throughout the construct at day 7. These data indicated that the flap construct became vascularized and obtained a blood supply quickly. The immediate blood perfusion through the pedicle is crucial to preventing ischemia in the flap immediately following implantation. We believe that the early perfusion and/or a short period of perfusion through the pedicle in the initial phase after implantation is critical to achieving optimal remodeling outcomes. This is because oxygen diffusion is limited, allowing only the cells within 100–200 μm of the nearest capillary to survive [40–42], and spontaneous vascular ingrowth into the implant usually takes several days to weeks [42]. Hence, ischemia/hypoxia always leads to necrosis or dysfunction of cells-biomaterials constructs and especially that of the core of large-scale engineered constructs. Unsurprisingly, then, we found in the present study that without reanastomosis to recipient vessels, even with precellularization, adipose tissue regeneration occurred only in the peripheral area of the explants in group B, whereas fibrosis occurred in most areas of the explant in both group B and group C. This finding coincides with previously reported clinical findings indicating that compared with non-vascularized free flap transplantation, vascularized adipose facial free flap transplantation results in better outcomes for patients undergoing facial contour deformity correction [43–44]. Unlike the constructs of groups B and C, the construct of group A was highly vascularized at 3 months, and this vascularization was closely associated with better constructive remodeling and maintenance of mature adipose tissue regeneration. Although the artery pedicle was obstructed, the vessels that originated in the surrounding tissue and those growing in the adventitia area provided the construct with adequate blood supply at this stage. Similar to the pathological process of vein graft disease [45–47], the shear stress on the engineered artery wall may have induced myointimal hyperplasia, resulting in lumen obstruction. In the present study, we used a static cell culture for DSAF repopulation; although this was appropriate for re-endothelialization, it may not deposit adequate ECM into the full layers of the artery wall to resist shear stress during re-perfusion. In future studies, therefore, we plan to use a dynamic long-term “organ culture” strategy to comprehensively improve the recellularization of DSAF and its vascular system especially [48]. In addition, because Microfil angiography only indirectly assessed the flap’s perfusion, our future studies may employ dynamic blood flow examination (e.g., Microfil injection with subsequent micro–computed tomography), which would provide a direct measure of flap perfusion in the early postoperative stage. Furthermore, although the main pedicle provided early blood perfusion

of the engineered flap construct and that this early perfusion played an important role in increasing the viability of the construct, the main pedicle lost patency within 7 days. At this point, the DSAF cannot really be considered a “true” flap. In particular, the sufficient vascularization of the center portion of the dermis may take longer than that of other areas of the implants, thereby resulting in the delayed remodeling. This may have been due to the subdermal vascular plexus not being completely open to allow blood to perfuse the dermis tissue, resulting in it behaving more like a graft. Maintaining the main pedicle’s patency for as long as possible—i.e., until the flap and the surrounding tissue have healed completely—is crucial for the DSAF’s survival in a clinical setting. Hence, encouraged by the success of this proof-of-concept study, we will focus on examining and increasing the patency of the main pedicle in future studies.

Studies have shown that a prefabrication approach to implanting a vascular pedicle into matrices could be used to successfully engineer a pedicle flap *in vivo* [49, 50]. In those studies and the present study, the close relationship between angiogenesis and adipogenesis are fully recognized. In the present study, however, we focused on engineering a free flap *ex vivo* to achieve more flexible applicability. The findings of the current study could be translated to large soft-tissue defect repair and reconstruction procedures such as breast augmentation and reconstruction. The decellularized dermis in the engineered composite soft tissue flap could provide support, whereas the acellular adipose tissue could drive adipose tissue regeneration. The peripheral sensory nerve structure in the flap matrix could easily bridge the host nerve growth into the flap. Indeed, we observed cellularization in the nerve structure after its end-to-side connection with the femoral nerve in the host; however, whether nerve function can fully recover in this setting requires further investigation [12, 51].

5. Conclusions

We used a perfusion-based protocol to produce DSAF with well-maintained ECM architecture that provided the molecular and topographical cues necessary for the integration and growth of hASCs and HUVECs. We demonstrated for the first time that this pre-vascularized, pre-cellularized dermal/adipose flap matrix, which included both a dominant vascular pedicle and microcirculatory network and integrated multiple types of cells, not only augments neovascularization but also modulates foreign-body reaction, thereby facilitating the constructive remodeling and long-term maintenance of adipose tissue regeneration. Our approach holds great promise for composite soft tissue free flap engineering and large-scale soft tissue repair and reconstruction.

Supplementary Material

Refer to Web version on PubMed Central for supplementary material.

Acknowledgments

This work was supported in part by the Kyte Foundation through MD Anderson’s Department of Plastic Surgery. This research was also supported by the National Institutes of Health through MD Anderson’s Cancer Center Support Grant P30CA016672 and used the High Resolution Electron Microscopy Facility and the Flow Cytometry and Cellular Imaging Core Facility. We thank Michael Gallagher in MD Anderson’s Department of Medical

Graphics & Photography for editing the Graphical Figure and Joseph Munch in MD Anderson's Department of Scientific Publications for editing the manuscript.

References

1. Shores JT, Brandacher G, Lee WP. Hand and upper extremity transplantation: an update of outcomes in the worldwide experience. Plast Reconstr Surg. 2015; 135:351e–60e.
2. Kueckelhaus M, Fischer S, Seyda M, Bueno EM, Aycart MA, Alhefzi M, ElKhal A, Pomahac B, Tullius SG. Vascularized composite allotransplantation: current standards and novel approaches to prevent acute rejection and chronic allograft deterioration. Transpl Int. 2015 Aug 12. [Epub ahead of print]. 10.1111/tri.12652
3. Siemionow M, Nasir S. Chimerism and bone marrow based therapies in transplantation. Microsurgery. 2007; 27:510–21. [PubMed: 17596895]
4. Siemionow M, Ortak T, Izycki D, Oke R, Cunningham B, Prajapati R, Zins JE. Induction of tolerance in composite-tissue allografts. Transplantation. 2002; 74:1211–7. [PubMed: 12451256]
5. Ott HC, Matthiesen TS, Goh SK, Black LD, Kren SM, Netoff TI, Taylor DA. Perfusion-decellularized matrix: using nature's platform to engineer a bioartificial heart. Nat Med. 2008; 14:213–21. [PubMed: 18193059]
6. Ott HC, Clippinger B, Conrad C, Schuetz C, Pomerantseva I, Ikonomou L, Kotton D, Vacanti JP. Regeneration and orthotopic transplantation of a bioartificial lung. Nat Med. 2010; 16:927–33. [PubMed: 20628374]
7. Uygun BE, Soto-Gutierrez A, Yagi H, Izamis ML, Guzzardi MA, Shulman C, Milwid J, Kobayashi N, Tilles A, Berthiaume F, Hertl M, Nahmias Y, Yarmush ML, Uygun K. Organ reengineering through development of a transplantable recellularized liver graft using decellularized liver matrix. Nat Med. 2010; 16:814–20. [PubMed: 20543851]
8. Mertsching H, Walles T, Hofmann M, Schanz J, Knapp WH. Engineering of vascularized scaffold for artificial tissue and organ generation. Biomaterials. 2005; 26:6610. [PubMed: 15979139]
9. Schultheiss D, Gabouev AI, Cebotari S, Tudorache I, Walles T, Schlote N, Wefer J, Kaufmann PM, Haverich A, Jonas U, Stief CG, Mertsching H. Biological vascularized matrix for bladder tissue engineering: matrix preparation, reseeding technique and short-term implantation in a porcine model. J Urol. 2005; 173:276–80. [PubMed: 15592096]
10. Mertsching H, Schanz J, Steger V, Schandar M, Schenk M, Hansmann J, Dally I, Friedel G, Walles T. Generation and transplantation of an autologous vascularized bioartificial human tissue. Transplantation. 2009(88):203. [PubMed: 19623015]
11. Aubin H, Kranz A, Hülsmann J, Pinto A, Barth M, Fomin A, Lichtenberg A, Akhyari P. A novel native derived coronary artery tissue-flap model. Tissue Eng Part C Methods. 2013; 19:970–80. [PubMed: 23631507]
12. Jank BJ, Xiong L, Moser PT, Guyette JP, Ren X, Cetrulo CL, Leonard DA, Fernandez L, Fagan SP, Ott HC. Engineered composite tissue as a bioartificial limb graft. Biomaterials. 2015; 61:246–56. [PubMed: 26004237]
13. Henderson PW, Nagineni VV, Harper A, Bavinck N, Sohn AM, Krijgh DD, Jimenez N, Weinstein AL, Spector JA. Development of an acellular bioengineered matrix with a dominant vascular pedicle. J Surg Res. 2010; 164:1–5. [PubMed: 20850792]
14. Qu J, Van Hogezand RM, Zhao C, Kuo BJ, Carlsen BT. Decellularization of a fasciocutaneous flap for use as a perfusable scaffold. Ann Plast Surg. 2015; 75:112–6. [PubMed: 24667881]
15. Wang L, Johnson JA, Zhang QX, Beahm EK. Combining decellularized human adipose tissue extracellular matrix and adipose-derived stem cells for adipose tissue engineering. Acta Biomater. 2013; 9:8921–31. [PubMed: 23816649]
16. Wang L, Johnson JA, Chang DW, Zhang QX. Decellularized musculofascial extracellular matrix for tissue engineering. Biomaterials. 2013; 34:2641–54. [PubMed: 23347834]
17. Zhang R, Ma PX. Poly(alpha-hydroxyl acids)/hydroxyapatite porous composites for bone-tissue engineering. I. Preparation and morphology. J Biomed Mater Res. 1999; 44:446–55. [PubMed: 10397949]

18. Flynn LE, Prestwich GD, Semple JL, Woodhouse KA. Adipose tissue engineering with naturally derived scaffolds and adipose-derived stem cells. Biomaterials. 2007; 28:3834–42. [PubMed: 17544502]
19. Flynn LE. The use of decellularized adipose tissue to provide an inductive microenvironment for the adipogenic differentiation of human adipose-derived stem cells. Biomaterials. 2010; 31:4715–24. [PubMed: 20304481]
20. Zuk PA, Zhu M, Mizuno H, Huang J, Futrell JW, Katz AJ, Benhaim P, Lorenz HP, Hedrick MH. Multilineage cells from human adipose tissue: implications for cell-based therapies. Tissue Eng. 2001; 7:211–28. [PubMed: 11304456]
21. Turner AE, Yu C, Bianco J, Watkins JF, Flynn LE. The performance of decellularized adipose tissue microcarriers as an inductive substrate for human adipose-derived stem cells. Biomaterials. 2012; 33:4490–9. [PubMed: 22456084]
22. Cukierman E, Pankov R, Stevens DR, Yamada KM. Taking cell-matrix adhesions to the third dimension. Science. 2001; 294:1708–12. [PubMed: 11721053]
23. Flynn LE, Prestwich GD, Semple JL, Woodhouse KA. Proliferation and differentiation of adipose-derived stem cells on naturally derived scaffolds. Biomaterials. 2008; 29:1862–71. [PubMed: 18242690]
24. Kwon YW, Heo SC, Jeong GO, Yoon JW, Mo WM, Lee MJ, Jang IH, Kwon SM, Lee JS, Kim JH. Tumor necrosis factor-alpha-activated mesenchymal stem cells promote endothelial progenitor cell homing and angiogenesis. Biochim Biophys Acta. 2013; 1832:2136–44. [PubMed: 23959047]
25. Hanson SE, D'Souza RN, Hematti P. Biomaterial-mesenchymal stem cell constructs for immunomodulation in composite tissue engineering. Tissue Eng Part A. 2014; 20:2162–8. [PubMed: 25140989]
26. Brown BN, Ratner BD, Goodman SB, Amar S, Badylak SF. Macrophage polarization: an opportunity for improved outcomes in biomaterials and regenerative medicine. Biomaterials. 2012; 33:3792–802. [PubMed: 22386919]
27. Brown BN, Valentin JE, Stewart-Akers AM, McCabe GP, Badylak SF. Macrophage phenotype and remodeling outcomes in response to biologic scaffolds with and without a cellular component. Biomaterials. 2009; 30:1482–91. [PubMed: 19121538]
28. Fishman JM, Lowdell MW, Urbani L, Ansari T, Burns AJ, Turmaine M, North J, Sibbons P, Seifalian AM, Wood KJ, Birchall MA, De Coppi P. Immunomodulatory effect of a decellularized skeletal muscle scaffold in a discordant xenotransplantation model. Proc Natl Acad Sci U S A. 2013; 110:14360–5. [PubMed: 23940349]
29. Faulk DM, Londono R, Wolf MT, Ranallo CA, Carruthers CA, Wildemann JD, Dearth CL, Badylak SF. ECM hydrogel coating mitigates the chronic inflammatory response to polypropylene mesh. Biomaterials. 2014; 35:8585–95. [PubMed: 25043571]
30. Morwood SR, Nicholson LB. Modulation of the immune response by extracellular matrix proteins. Arch Immunol Ther Exp (Warsz). 2006; 54:367–74. [PubMed: 17122884]
31. Thomas AH, Edelman ER, Stultz CM. Collagen fragments modulate innate immunity. Exp Biol Med (Maywood). 2007; 232:406–11. [PubMed: 17327474]
32. Bollyky PL, Falk BA, Wu RP, Buckner JH, Wight TN, Nepom GT. Intact extracellular matrix and the maintenance of immune tolerance: High molecular weight hyaluronan promotes persistence of induced CD4+CD25+ regulatory T cells. J Leukoc Biol. 2009; 86:567–72. [PubMed: 19401397]
33. Hanson SE, King SN, Kim J, Chen X, Thibeault SL, Hematti P. The effect of mesenchymal stromal cell-hyaluronic acid hydrogel constructs on immunophenotype of macrophages. Tissue Eng Part A. 2011; 17:2463–71. [PubMed: 21554192]
34. King SN, Hanson SE, Chen X, Kim J, Hematti P, Thibeault SL. In vitro characterization of macrophage interaction with mesenchymal stromal cell-hyaluronan hydrogel constructs. J Biomed Mater Res A. 2014; 102:890–902. [PubMed: 23564555]
35. Vallés G, Bensiamar F, Crespo L, Arruebo M, Vilaboa N, Saldaña L. Topographical cues regulate the crosstalk between MSCs and macrophages. Biomaterials. 2014; 37:124–33. [PubMed: 25453943]
36. Moyer AL, Wagner KR. Regeneration versus fibrosis in skeletal muscle. Curr Opin Rheumatol. 2011; 23:568–73. [PubMed: 21934499]

37. Han TT, Toutounji S, Amsden BG, Flynn LE. Adipose-derived stromal cells mediate in vivo adipogenesis, angiogenesis and inflammation in decellularized adipose tissue bioscaffolds. Biomaterials. 2015; 72:125–37. [PubMed: 26360790]
38. Sun X, Kang Y, Bao J, Zhang Y, Yang Y, Zhou X. Modeling vascularized bone regeneration within a porous biodegradable CaP scaffold loaded with growth factors. Biomaterials. 2013; 34:4971–81. [PubMed: 23566802]
39. Laco F, Grant MH, Black RA. Collagen-nanofiber hydrogel composites promote contact guidance of human lymphatic microvascular endothelial cells and directed capillary tube formation. J Biomed Mater Res A. 2013; 101:1787–99. [PubMed: 23197422]
40. Lovett M, Lee K, Edwards A, Kaplan DL. Vascularization strategies for tissue engineering. Tissue Eng Part B Rev. 2009; 15:353–70. [PubMed: 19496677]
41. Velazquez OC. Angiogenesis and vasculogenesis: inducing the growth of new blood vessels and wound healing by stimulation of bone marrow-derived progenitor cell mobilization and homing. J Vasc Surg. 2007; 45:A39–47. [PubMed: 17544023]
42. Rouwkema J, Rivron NC, van Blitterswijk CA. Vascularization in tissue engineering. Trends Biotechnol. 2008; 26:434–41. [PubMed: 18585808]
43. Wang X, Qiao Q, Liu Z, Zhao R, Zhang H, Yang Y, Wang Y, Bai M. Free anterolateral thigh adipofascial flap for hemifacial atrophy. Ann Plast Surg. 2005; 55:617–22. [PubMed: 16327463]
44. Zhang Q, Qiao Q, Zhou G, Robb GL. Anterolateral thigh adipofascial flap for correction of facial contour deformities and micromastia. J Reconstr Microsurg. 2010; 26:341–5. [PubMed: 20183785]
45. Lu DY, Chen EY, Wong DJ, Yamamoto K, Protack CD, Williams WT, Assi R, Hall MR, Sadaghianloo N, Dardik A. Vein graft adaptation and fistula maturation in the arterial environment. J Surg Res. 2014; 188:162–73. [PubMed: 24582063]
46. Anwar MA, Shalhoub J, Lim CS, Gohel MS, Davies AH. The effect of pressure-induced mechanical stretch on vascular wall differential gene expression. J Vasc Res. 2012; 49:463–78. [PubMed: 22796658]
47. Chiu JJ, Chien S. Effects of disturbed flow on vascular endothelium: pathophysiological basis and clinical perspectives. Physiol Rev. 2011; 91:327–87. [PubMed: 21248169]
48. Rennert RC, Sorkin M, Wong VW, Gurtner GC. Organ-level tissue engineering using bioreactor systems and stem cells: implications for transplant surgery. Curr Stem Cell Res Ther. 2014; 9:2–9. [PubMed: 24180421]
49. Dolderer JH, Thompson EW, Slavin J, Trost N, Cooper-White JJ, Cao Y, O'Connor AJ, Penington A, Morrison WA, Abberton KM. Long-term stability of adipose tissue generated from a vascularized pedicled fat flap inside a chamber. Plast Reconstr Surg. 2011; 127:2283–92. [PubMed: 21617462]
50. Zhang Q, Hubenak J, Iyyanki T, Alred E, Turza KC, Davis G, Chang EI, Branch-Brooks CD, Beahm EK, Butler CE. Engineering vascularized soft tissue flaps in an animal model using human adipose-derived stem cells and VEGF+PLGA/PEG microspheres on a collagen-chitosan scaffold with a flow-through vascular pedicle. Biomaterials. 2015; 73:198–213. [PubMed: 26410787]
51. Szynkaruk M, Kemp SW, Wood MD, Gordon T, Borschel GH. Experimental and clinical evidence for use of decellularized nerve allografts in peripheral nerve gap reconstruction. Tissue Eng Part B Rev. 2013; 19:83–96. [PubMed: 22924762]

Statement of significance

Significant soft tissue loss resulting from traumatic injury or tumor resection often requires surgical reconstruction using autologous soft tissue flaps. However, the limited availability of qualitative autologous flaps as well as the donor site morbidity significantly limits this approach. Engineered soft tissue flap grafts may offer a clinically relevant alternative to the autologous flap tissue. In this study, we engineered vascularized soft tissue free flap by using skin/adipose flap extracellular matrix scaffold (DSAF) in combination with multiple types of human cells. Following vascular reanastomosis in the recipient site, the engineered products successful regenerated large-scale fat tissue *in vivo*. This approach may provide a translatable platform for composite soft tissue free flap engineering for microsurgical reconstruction.

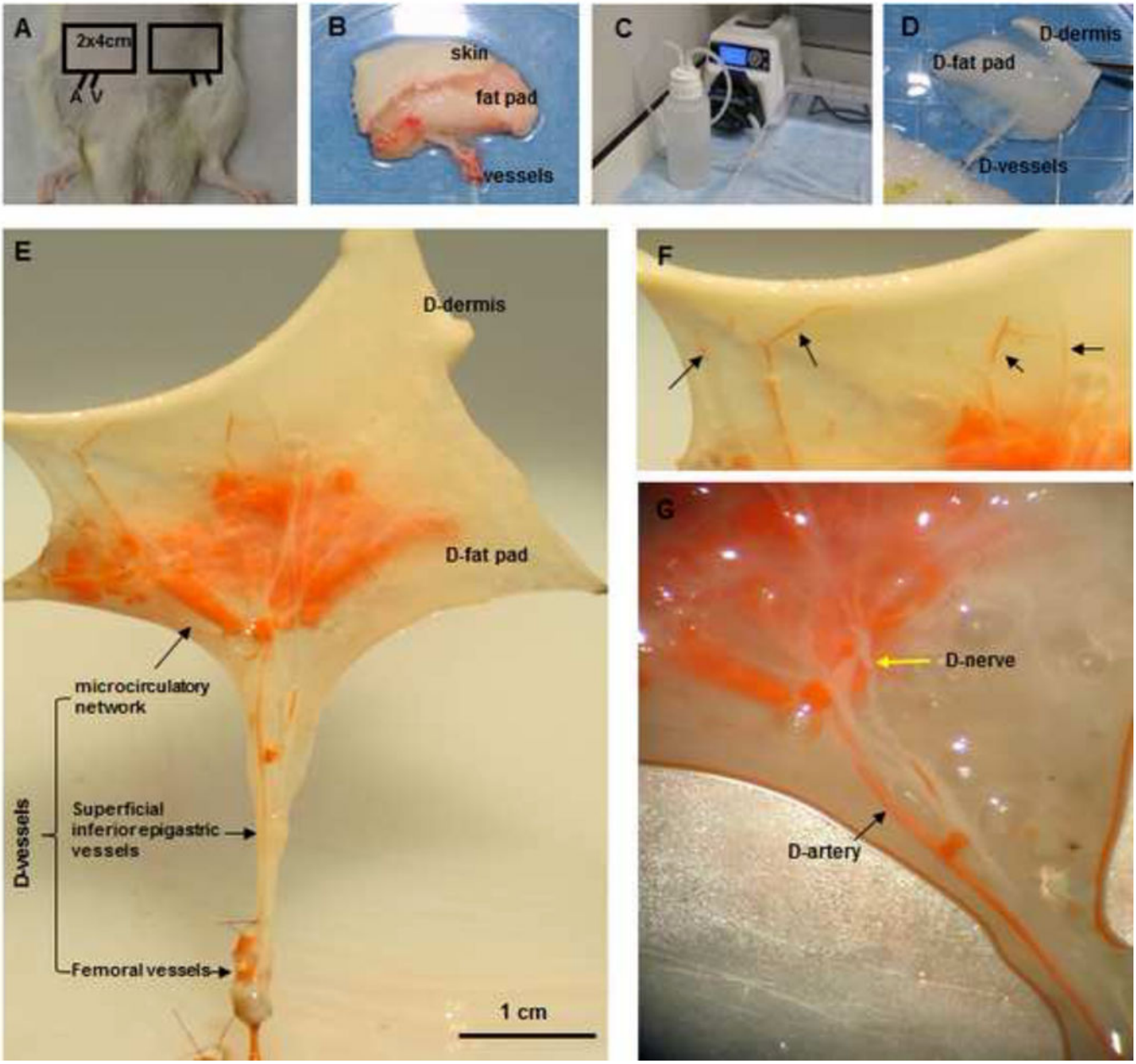

Fig. 1. Perfusion decellularization and flap matrix angiography

(A, B) Groin skin/adipose tissue flaps with vascular pedicles (2 cm × 4 cm) were harvested from Fischer 344 rats. (C, D) Transparent DSAF matrix was achieved using a bump perfusion system combined with agitation decellularization. ("D-" indicates "decellularized" in this and other figures.) (E) Microfil-117 angiography showed that DSAF retained femoral vessels, superficial inferior epigastric vessels, and microcirculatory vessels. (F) Artery perforators penetrated into the dermis (black arrows). (G) An acellular sensory nerve (yellow arrow) and artery (black arrow) are shown.

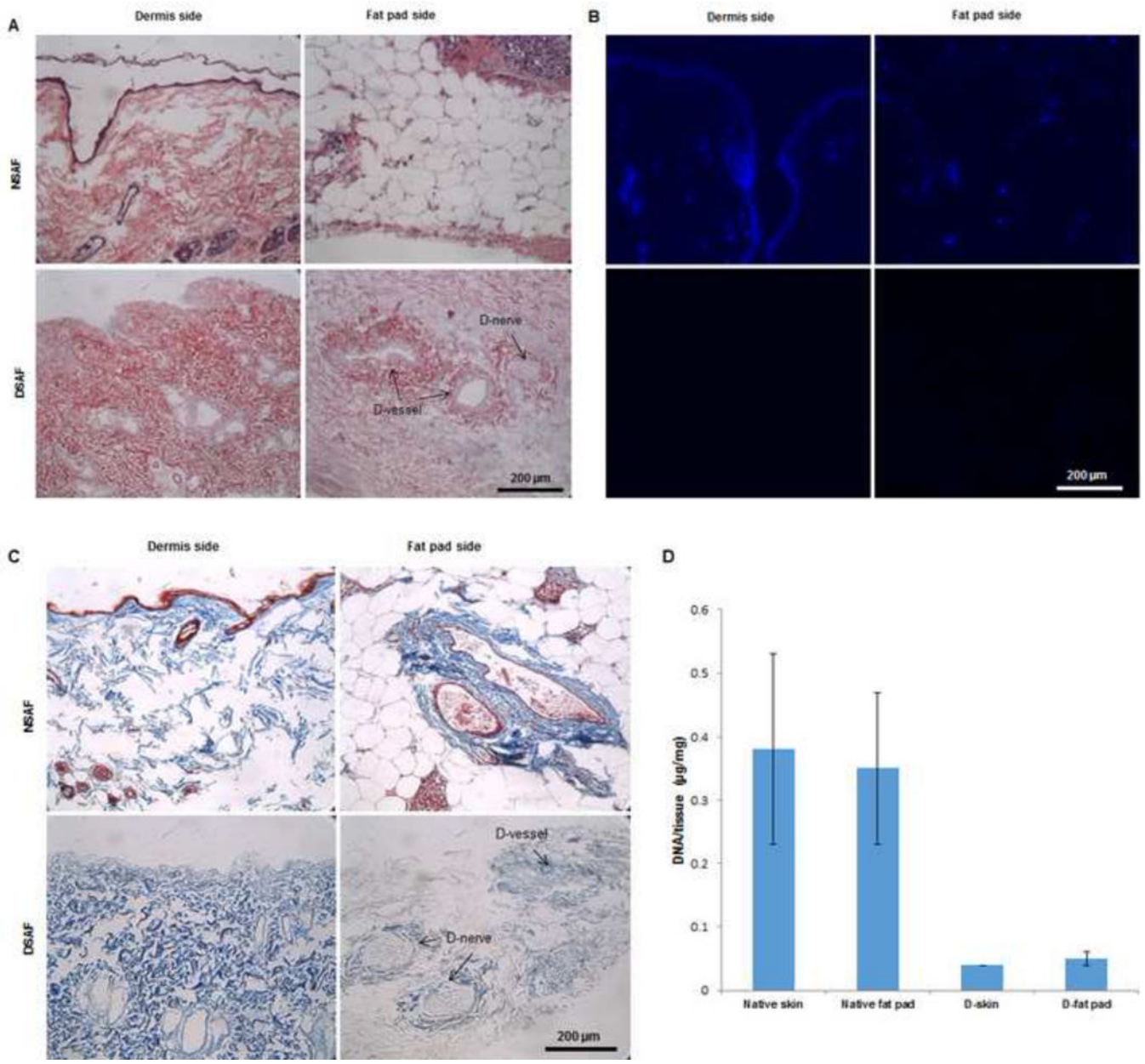

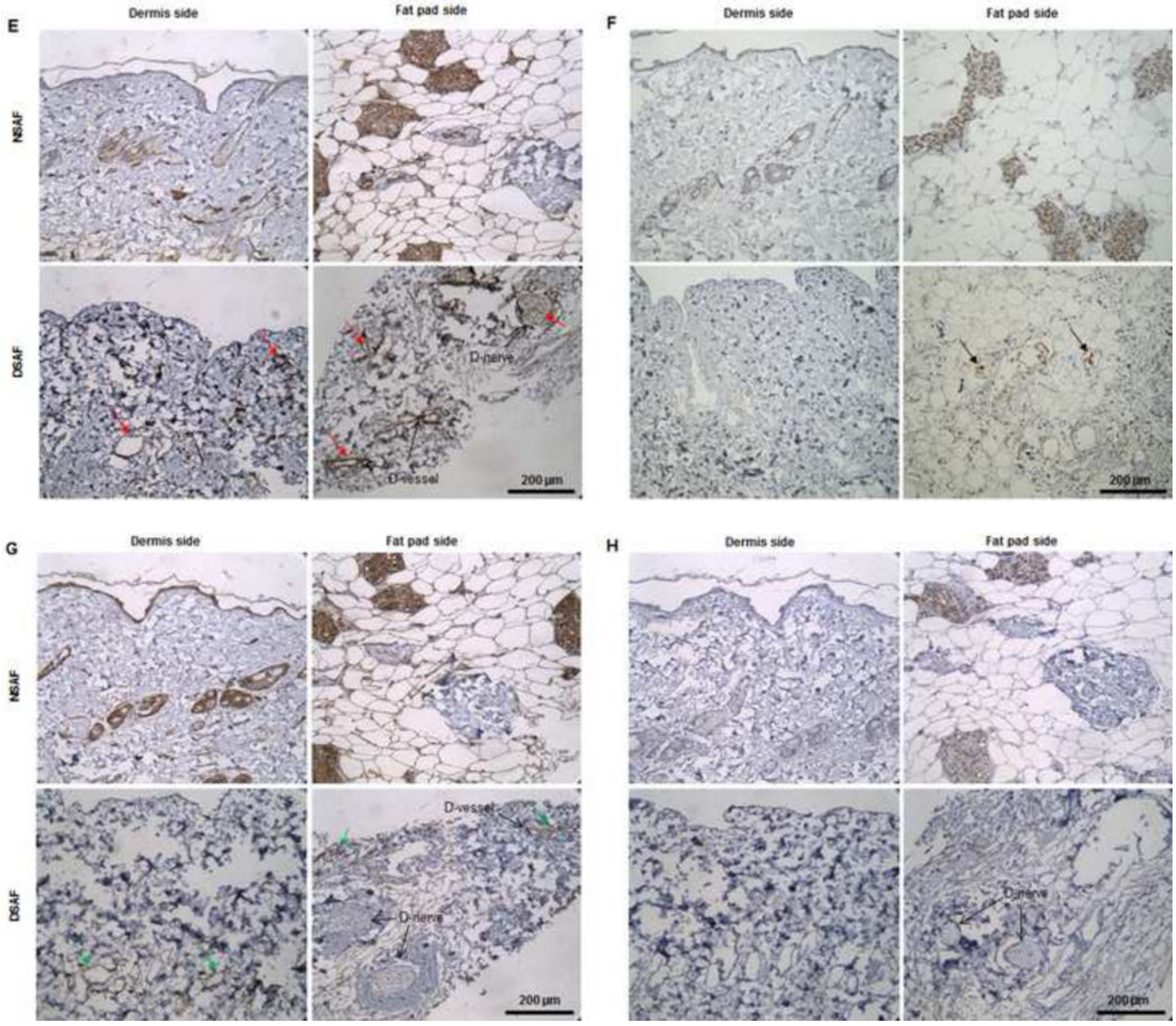

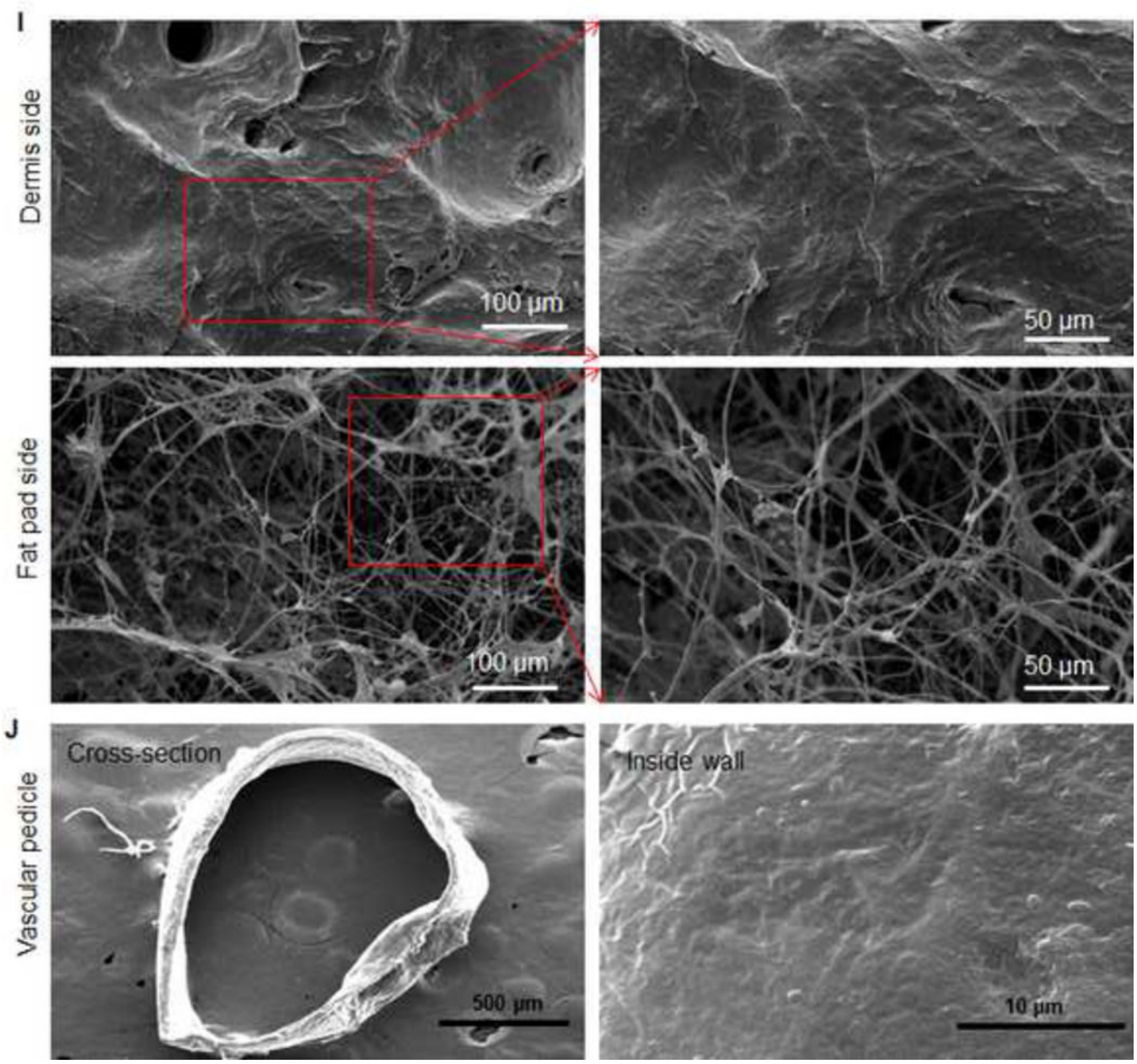

Fig. 2. Characterization of DSAF

(A) H&E staining showed that blood vessels and nerve structures were well maintained in DSAF. Cell nuclei were present in NSAF but absent in DSAF. (B) DAPI staining revealed the absence of nuclei DNA in DSAF. (C) Masson trichrome staining showed that collagen was a major component of DSAF. (D) The DNA content in the decellularized skin and fat pad was significantly lower than that in the native skin and fat pad ($P<0.05$). (E) IHC analysis indicated that laminin was distributed in vessels, nerves, and nanofibrous structures in DSAF (red arrows). (F) bFGF was present in the glandular and nanofibrous structures of DSAF (black arrows). (G) VEGF was present in the vessels and nerve structures of DSAF (green arrows). (H) The absence of MHC-I indicated the removal of alloantigenicity from

DSAF. (I) SEM images confirmed that cells were absent in DSAF, leaving 3D porous structures in the fat pad side. Nanofibrous structures of ECM were well maintained in DSAF. (J) SEM images showed that the decellularized femoral artery remained elastic and patent.

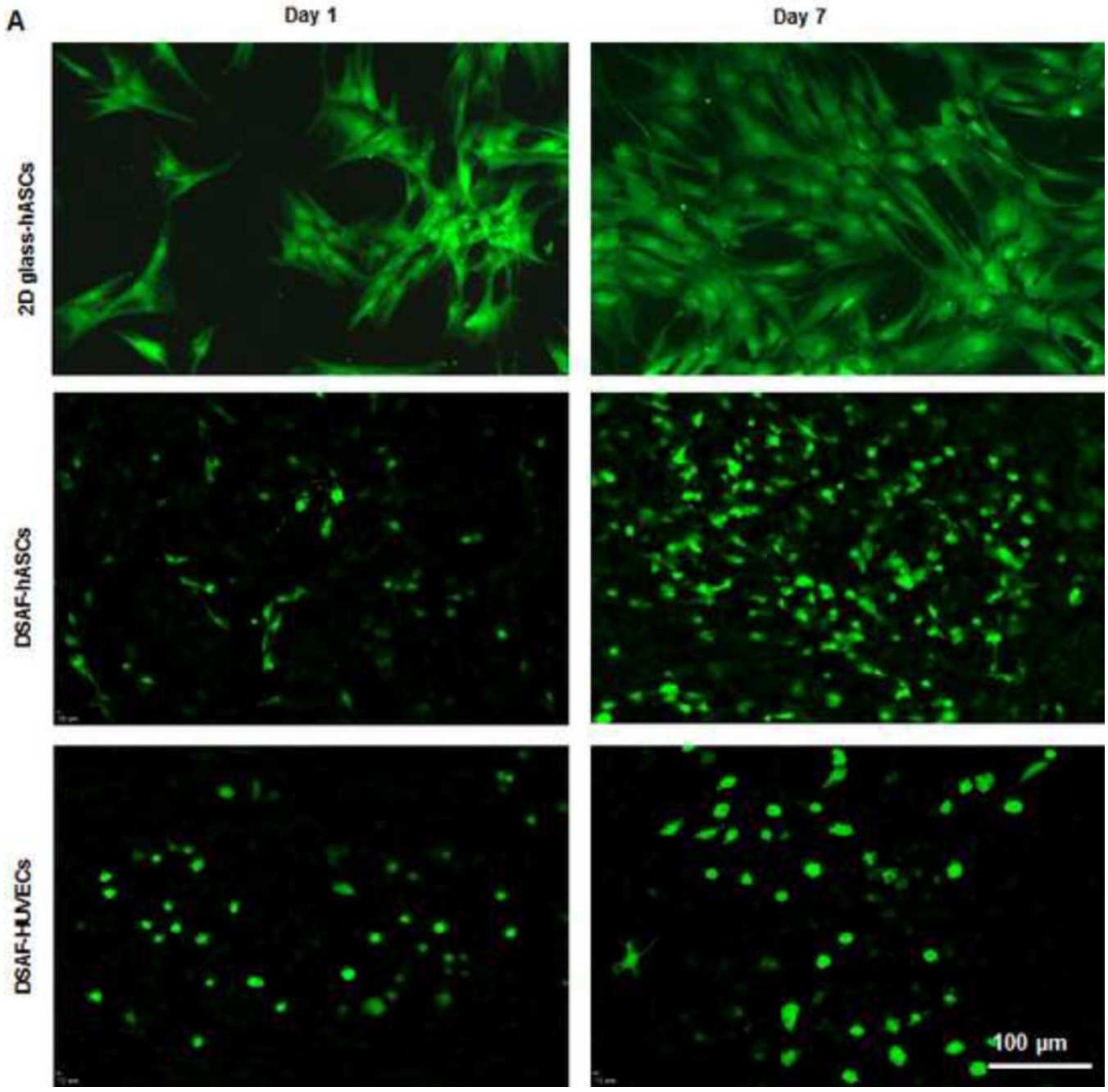

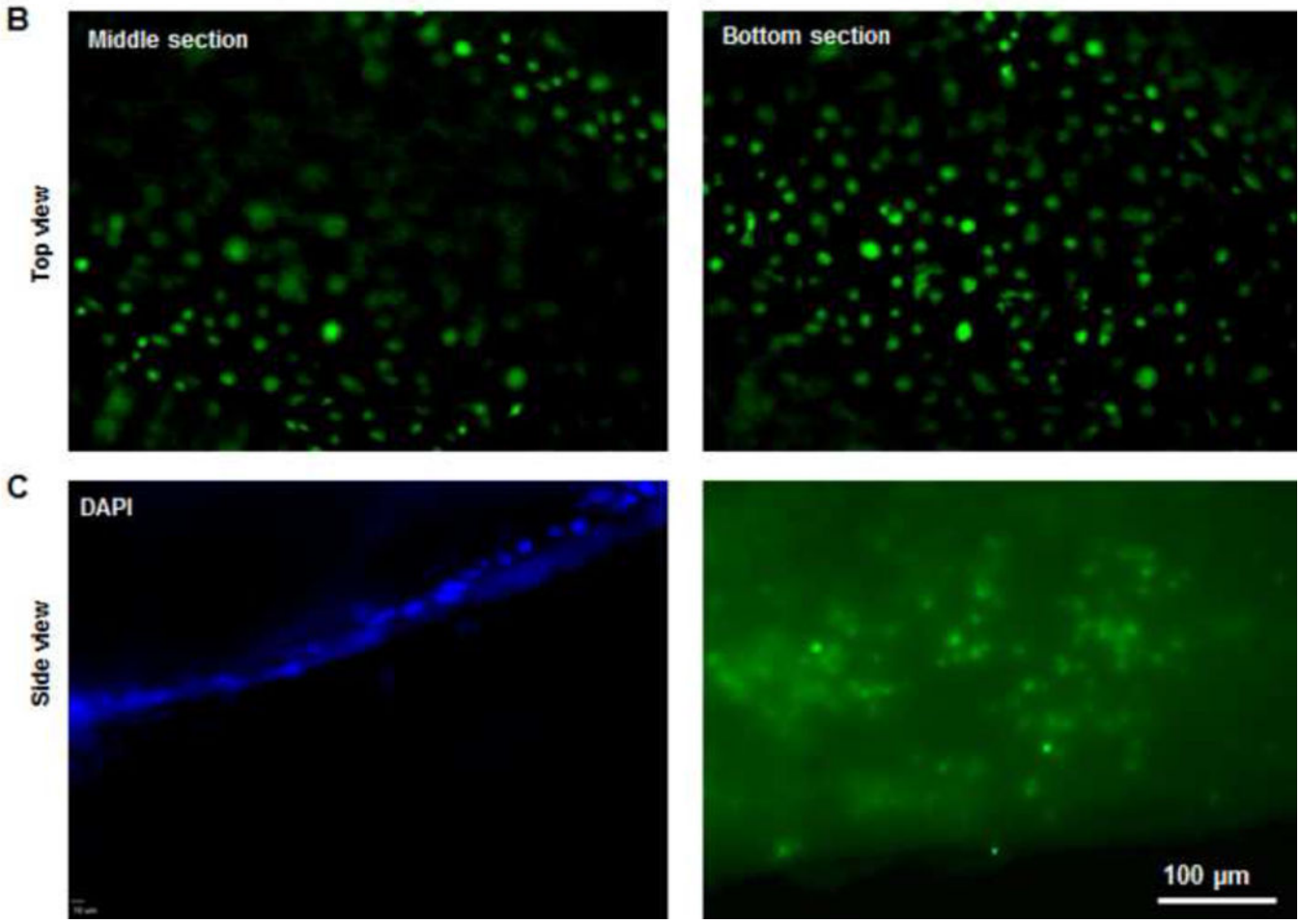

Fig. 3. Recellularization of DSAF

(A) Confocal microscopy images showed hASCs and HUVECs on DSAF. Cells were stained with Calcein AM (green) and EthD-1 (red) on days 1 and 7 after seeding. (B) Confocal microscopy images of HUVECs integrated with the DSAF pedicle (top view). (C) Confocal (DAPI staining) and fluorescence (Calcein AM and EthD-1 staining) microscopy images of HUVECs integrated with the DSAF pedicle (side view).

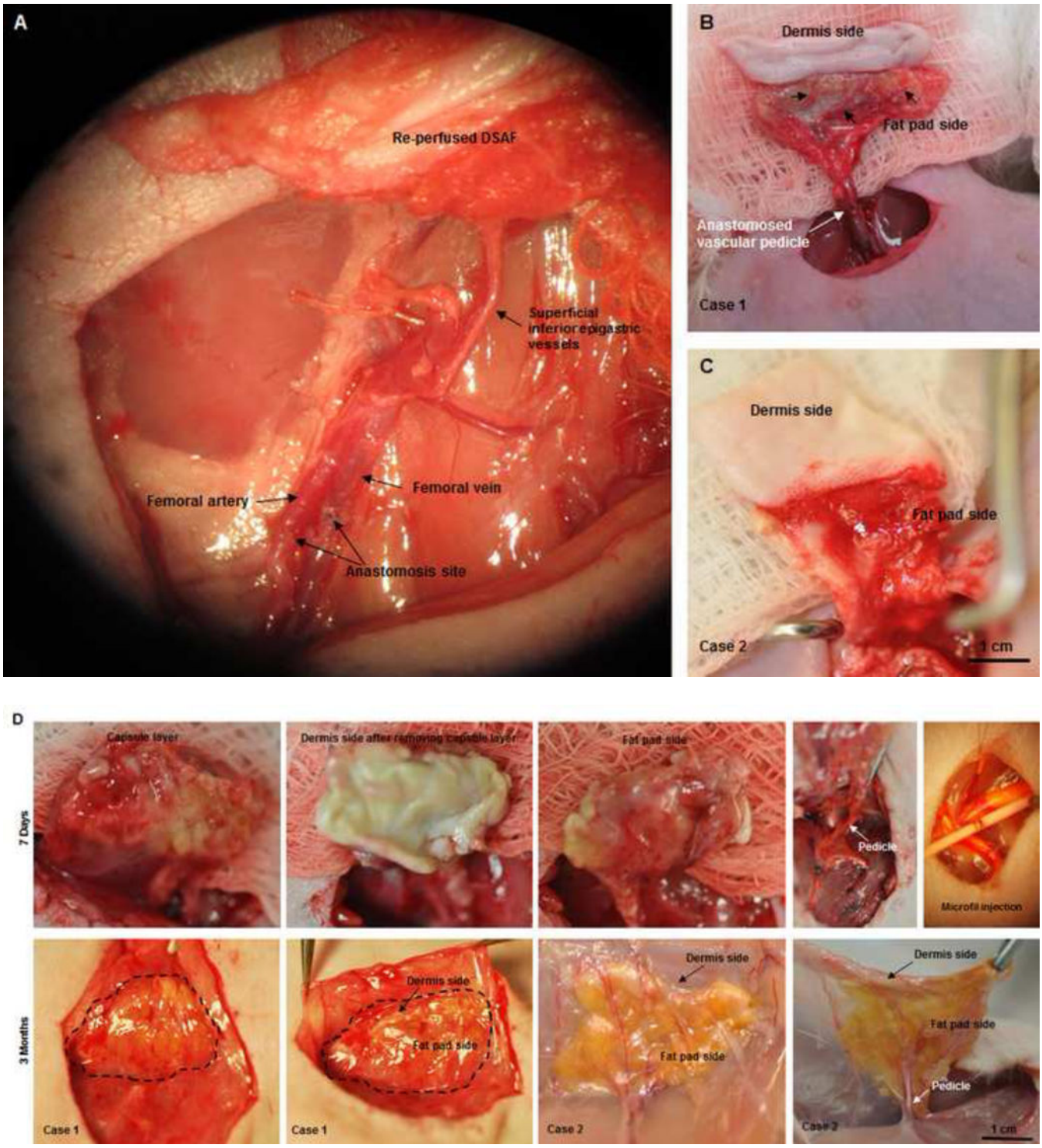

Fig. 4. Implantation and explantation of the engineered DSAF-cells construct in group A

(A) The vascular pedicle was re-integrated into the host using conventional microsurgical anastomosis techniques. (B, C) Blood immediately perfused the engineered flap construct. (D) At 7 days (top row), the implant was encapsulated in swollen tissue (first image). Removing the swollen tissue capsule from the fat pad resulted in bleeding (second and third

images). Mircofil-117 went through the vascular pedicle (fourth image) when it was injected through the contralateral femoral artery at day 7 (fifth image). At 3 months (bottom row), the implant was remodeled. Adipose tissue formed on both the dermis side and fat pad side. Numerous visible blood vessels penetrated into the newly formed soft tissue, indicating that it was highly vascularized.

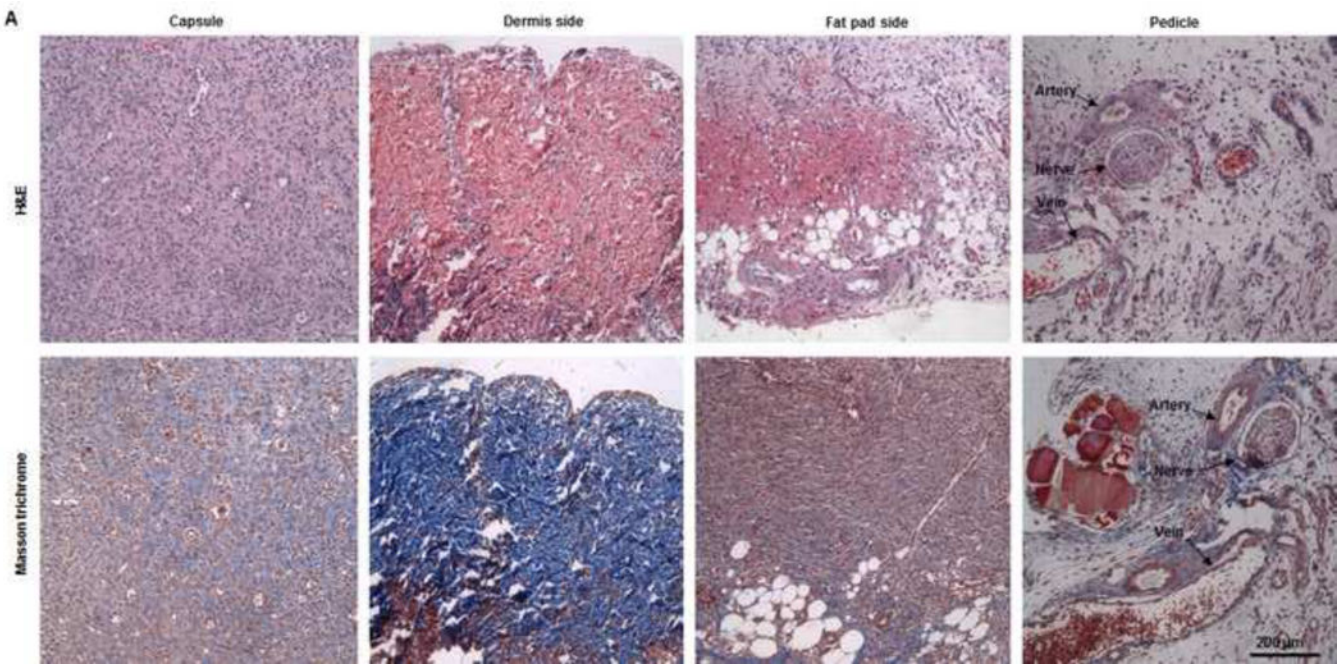

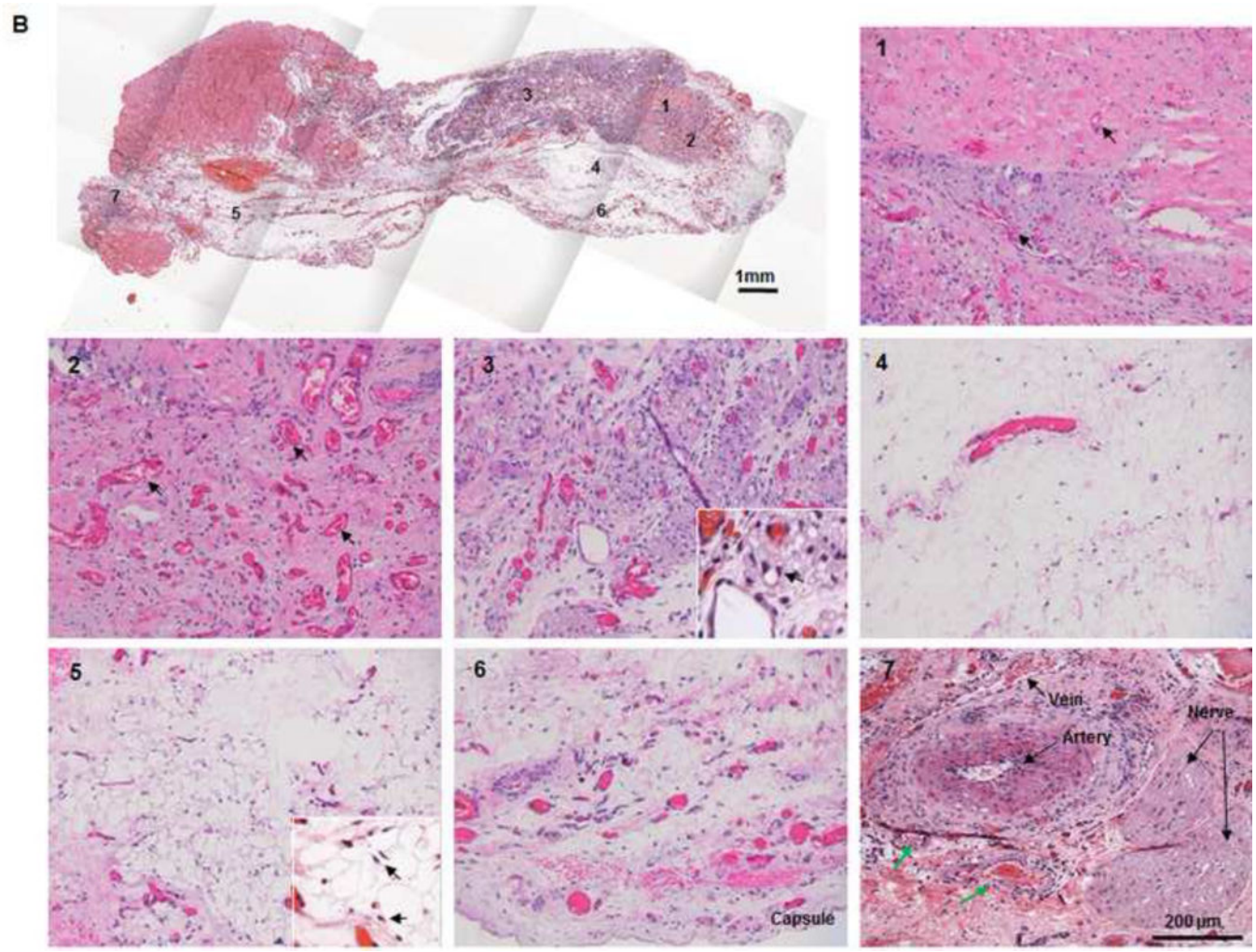

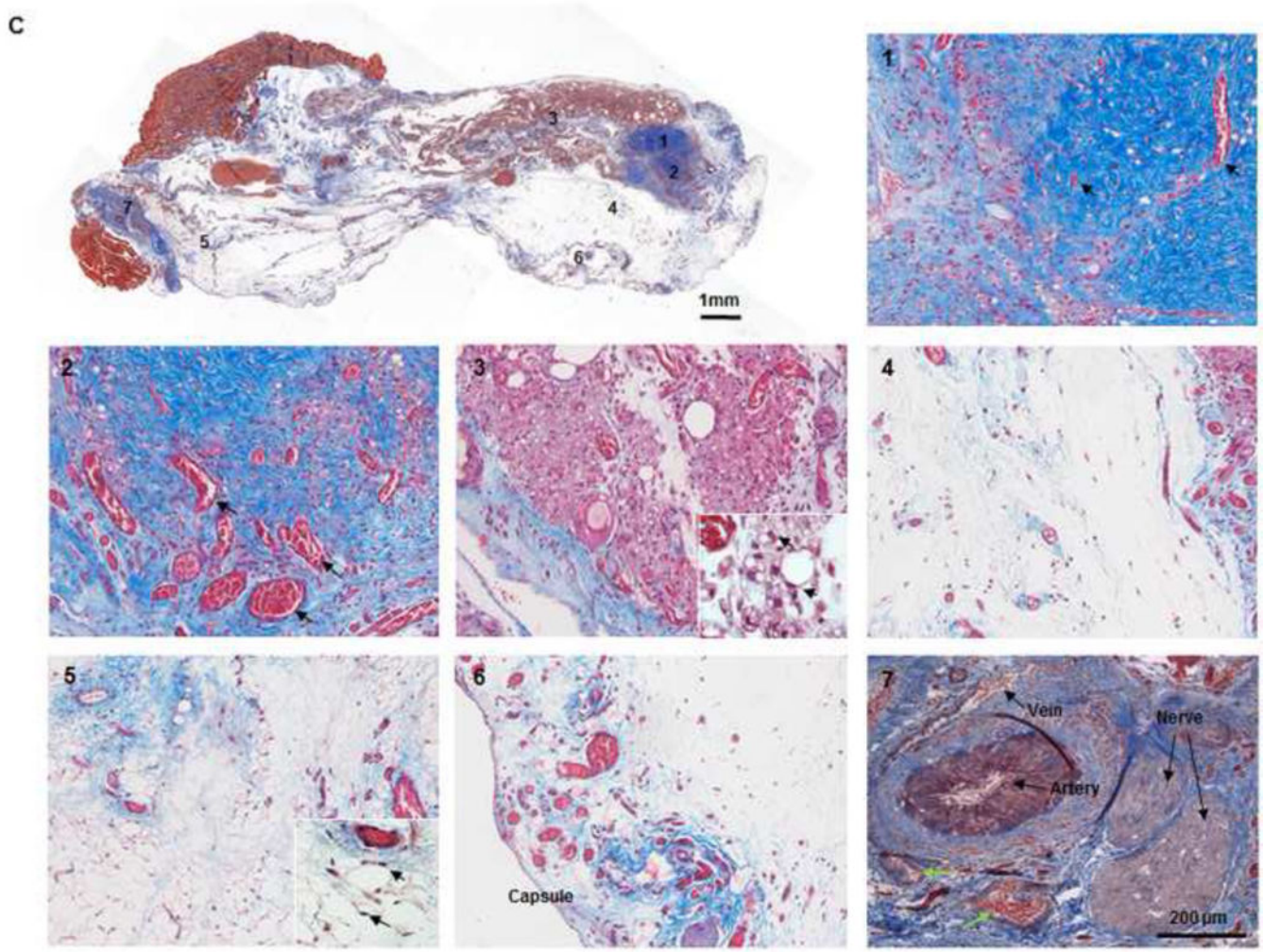

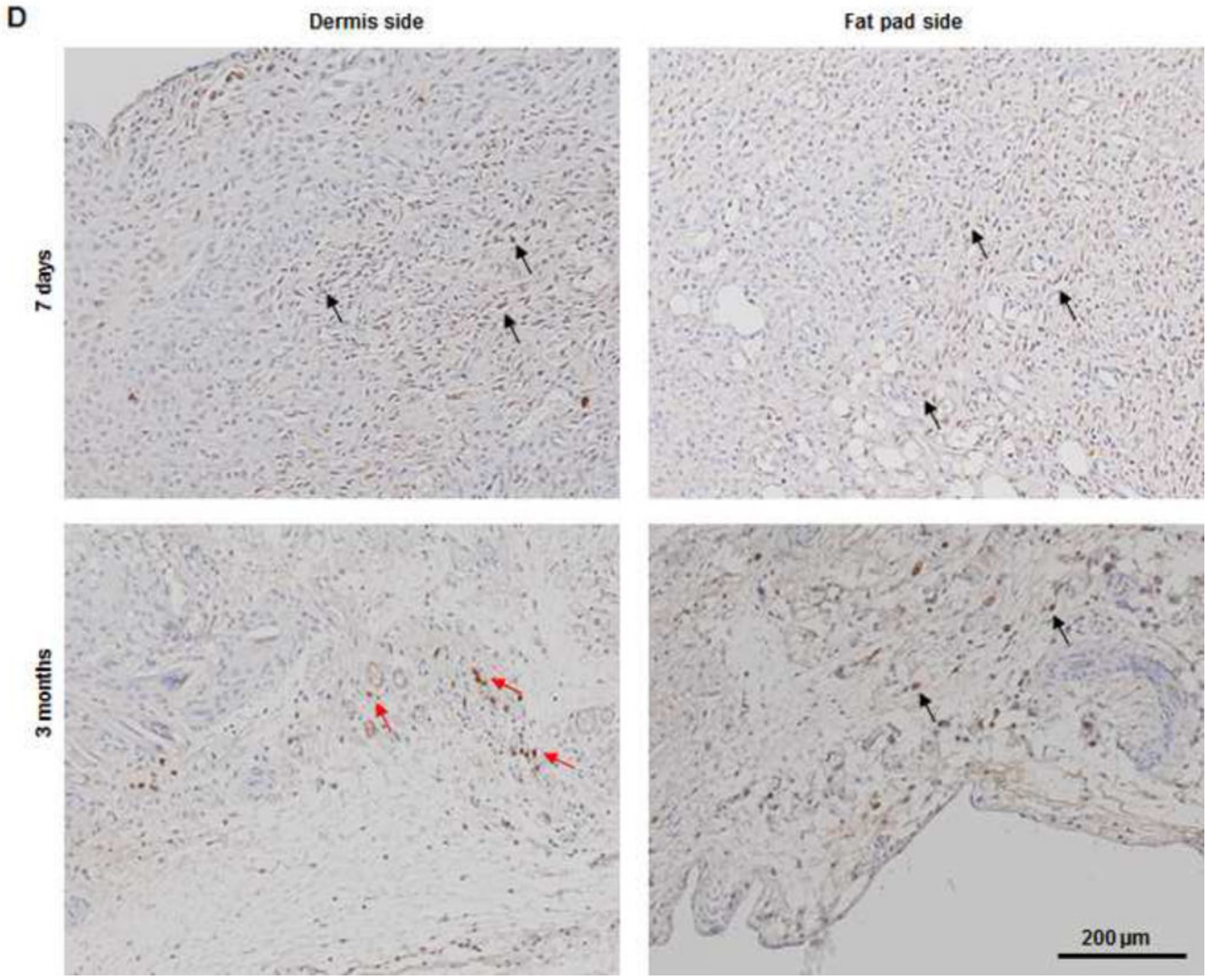

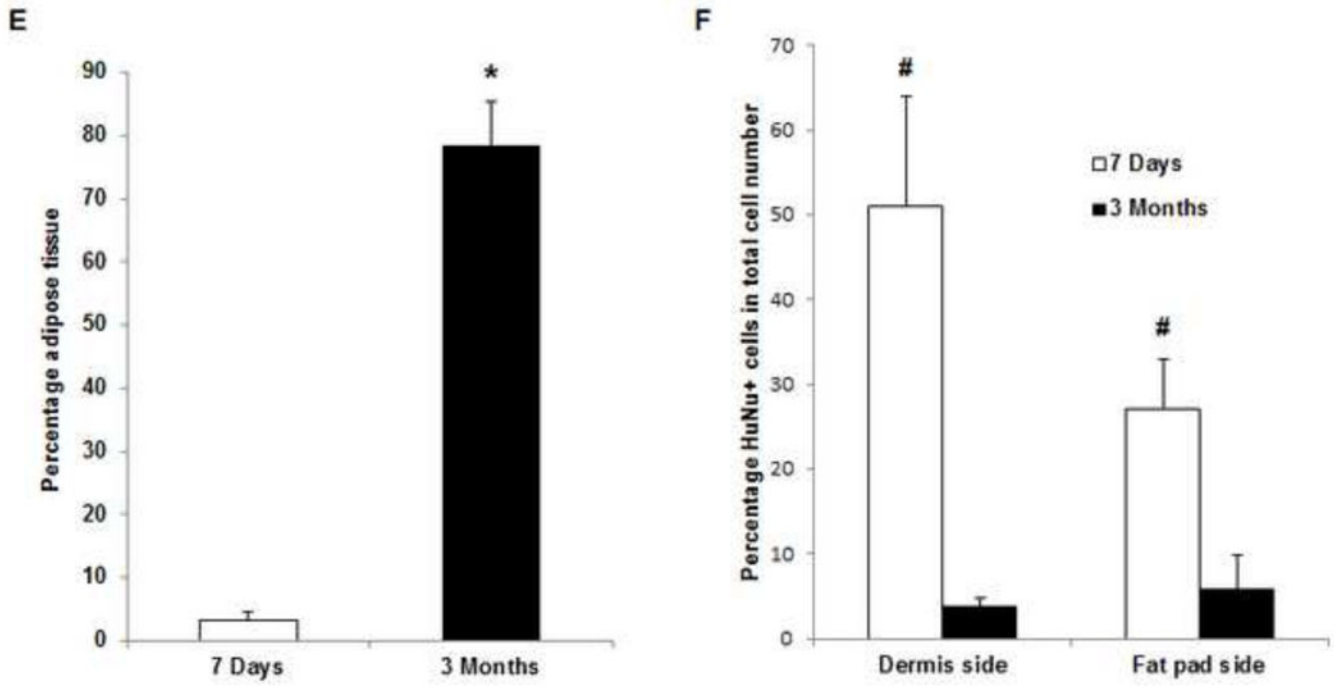

Fig. 5. Histological analysis of explants in group A

(A) H&E and Masson trichrome staining revealed an inflammation reaction characterized by cellular and vascular infiltration in the tissue at day 7. Lots of intravascular red blood cells were within the large-diameter blood vessels in the pedicle area. (B, C) H&E and Masson trichrome staining showed constructive remodeling in the implant at 3 months. Most dermis tissue was degraded and remodeled as adipose fascial tissue, and a small portion of dense collagen remained. The fat pad side of the implanted flap construct was fully remodeled, showing mature adipose tissue formed by adipocyte cells. (The numbered areas in the top images are magnified in the correspondingly numbered bottom images). The center of the dermis (images 1&2) was undergoing constructive remodeling, with dense collagen, highly vascular infiltration (black arrows), and numerous adipocytes. The outer layer of the dermis (image 3) showed a high level of remodeling, with numerous proliferating adipocytes (black arrows), blood vessel formation, and collagen that was less dense than that in the center of the dermis. The fat pad side of the construct (images 4–6) was completely remodeled, showing mature adipose tissue (black arrows), loose fascial tissue, a high number of blood vessels, and no inflammatory cells. In the pedicle area of the construct (image 7), myointimal hyperplasia of the main artery was present, the vein was patent, a number of functional vessels grew (green arrows), and the intact sensory nerve structure was recellularized. (D) The presence of donor cells was evaluated by immunohistochemical staining for an anti-HuNu antibody. HuNu-positive cells were distinguishable and persistent at 7 days and 3 months. Donor cells were closely located around the vascular structures (red arrow) and adipose structures (black arrow) at 3 months. (E) The area of adipose tissue at 3 months was significantly greater than that at 7 days. *: $P<0.05$ as compared to 7 days. (F) There were significantly fewer HuNu-positive cells at 3 months than at 7 days. The percentage of donor cells at 3 months was significantly lower than that at 7 days. #: $P<0.05$ as compared to 3 months.

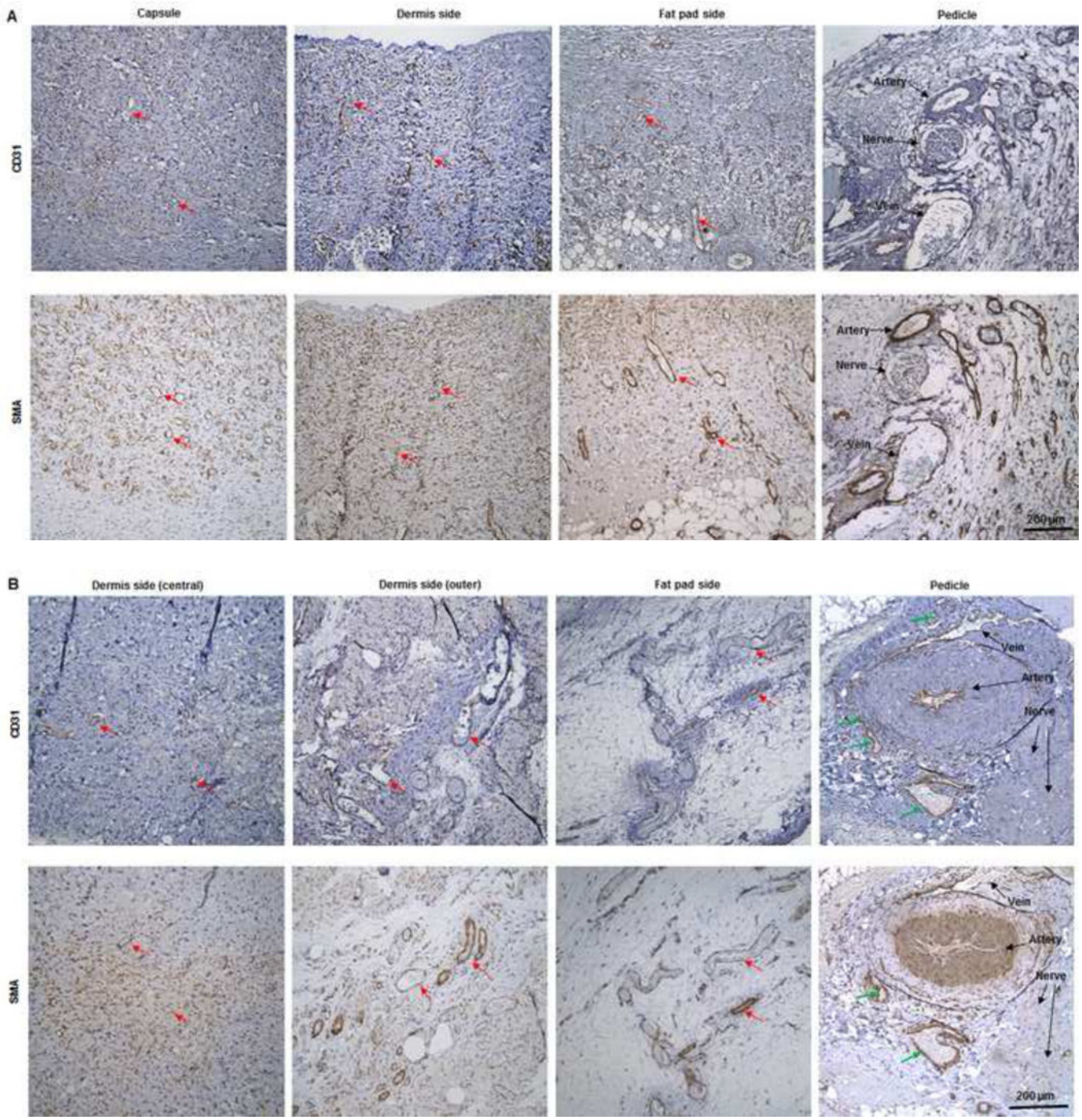

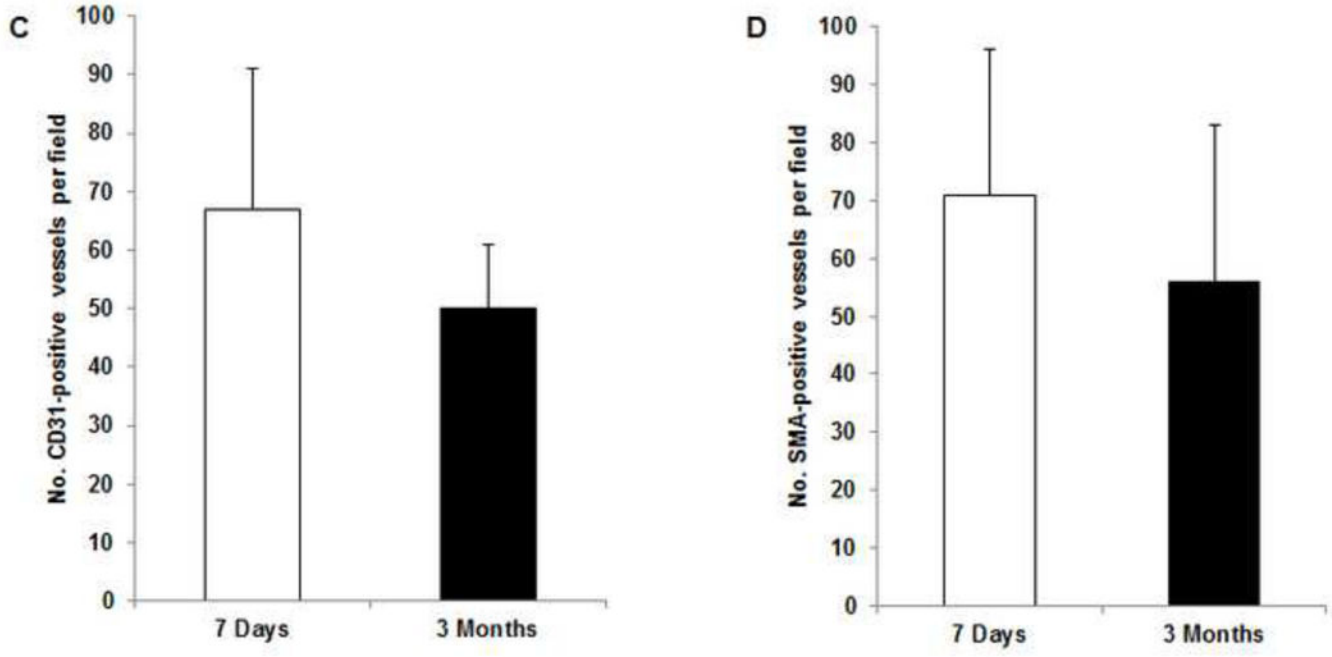

Fig. 6. IHC analysis of explants in group A

(A) Abundant CD31- and SMA-positive blood vessels were distributed in the capsule, dermis, and fat pad area of the explant (red arrows) at day 7. (B) The adipose tissue was highly vascularized, showing numerous CD31- and SMA-positive vessels (red arrows) throughout the explant at 3 months; lots of red blood cells were present in the functional vessels. Although the main pedicle artery showed myointimal hyperplasia, lots of vessels grew in the adventitia area (green arrows). (C&D) The numbers of CD31-positive vessels and SMA-positive vessels at 7 days and 3 months were both large and did not differ significantly.

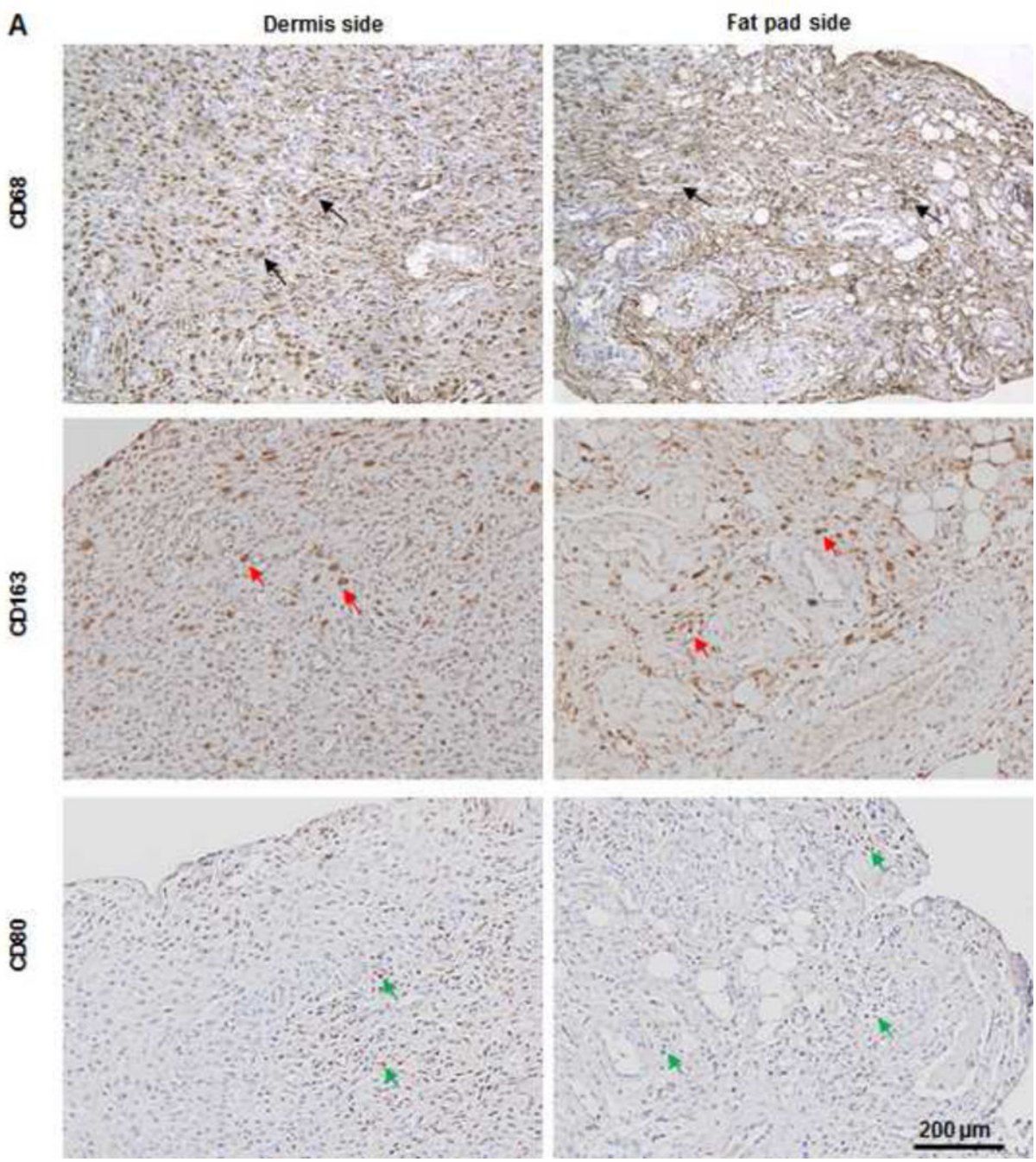

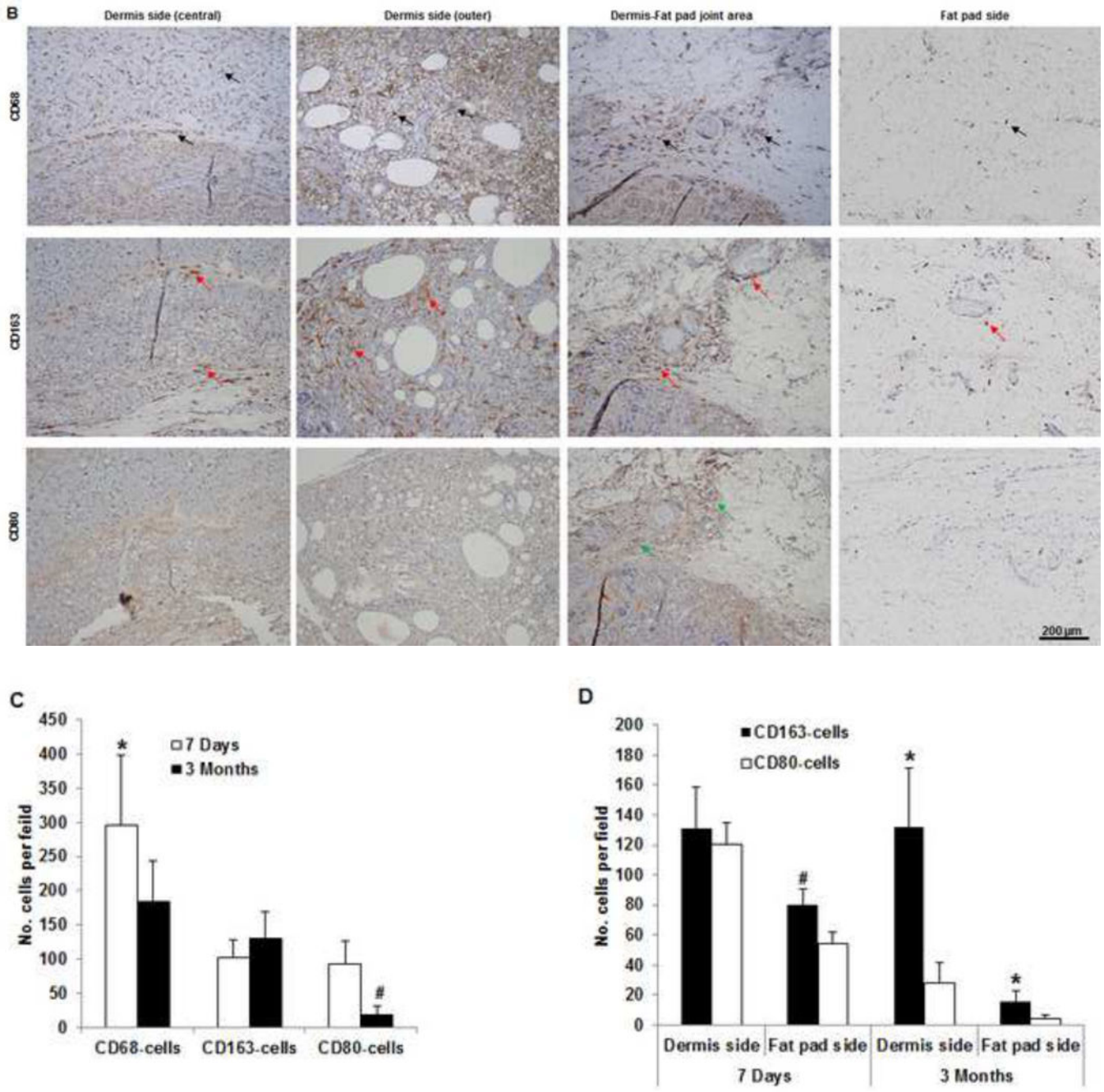

Fig. 7. IHC analysis of explants in group A

(A) As predominant inflammatory cells, many CD68-positive macrophages (black arrows) infiltrated the construct at day 7. Among these cells, both CD80-positive macrophages (M1 macrophages; green arrows) and CD163-positive macrophages (M2 macrophages; red arrows) were found throughout the sample tissue. (B) There were significantly fewer CD68-positive macrophages (black arrows) and CD80-positive macrophages (green arrows) at 3 months than at 7 days. Most macrophages were CD163-positive M2 macrophages (red arrows), which predominantly infiltrated the dermis side. Much fewer inflammatory

macrophages were present in the fat pad side, indicating that the area was fully remodeled. (C) There were significantly fewer CD68- and CD80-positive macrophages at 3 the fat pad side at 7 days and in both the dermis and fat pad side at 3 months. *: $P<0.05$ as compared to CD80; #: $P<0.05$ as compared to CD80.

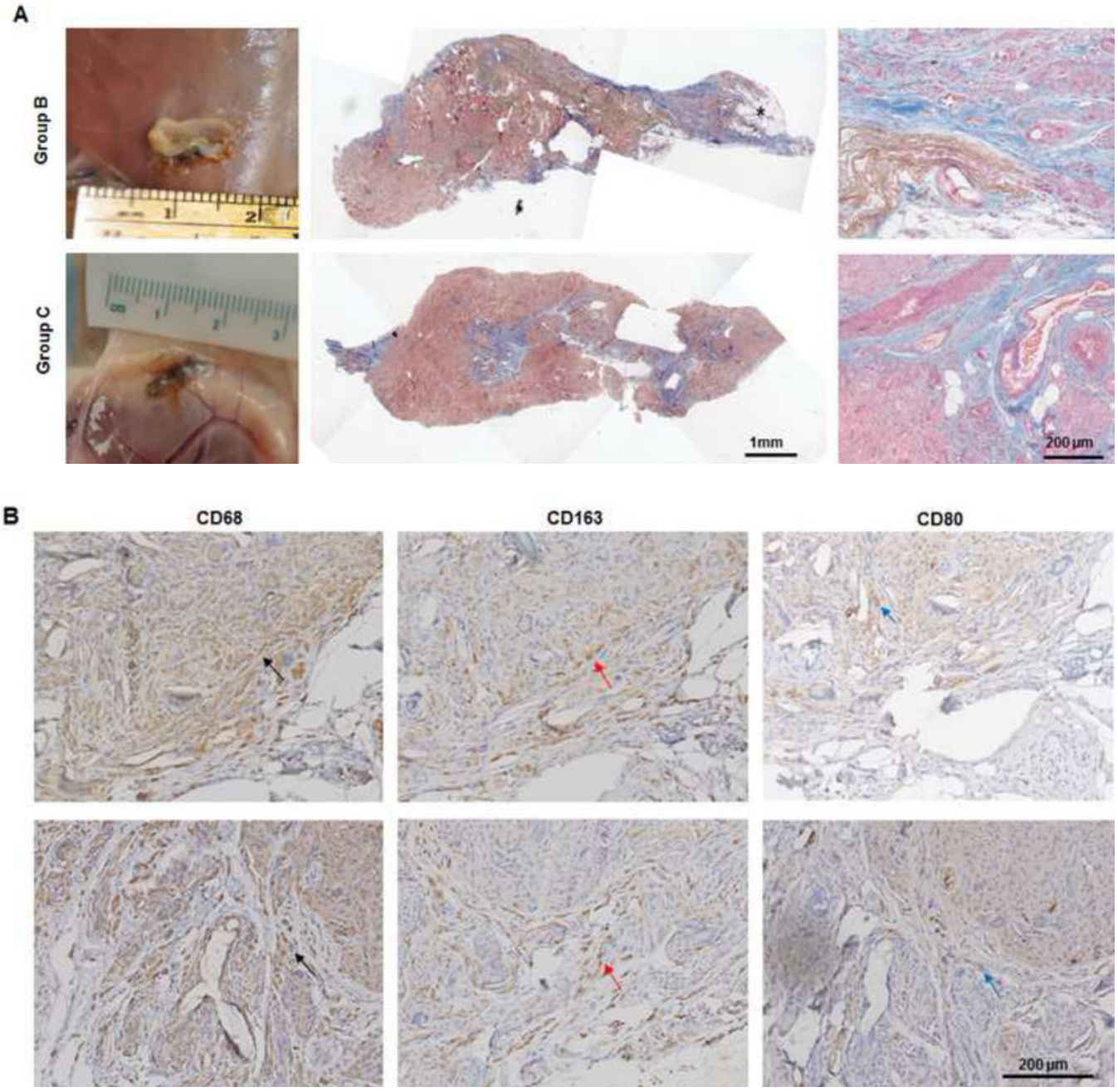

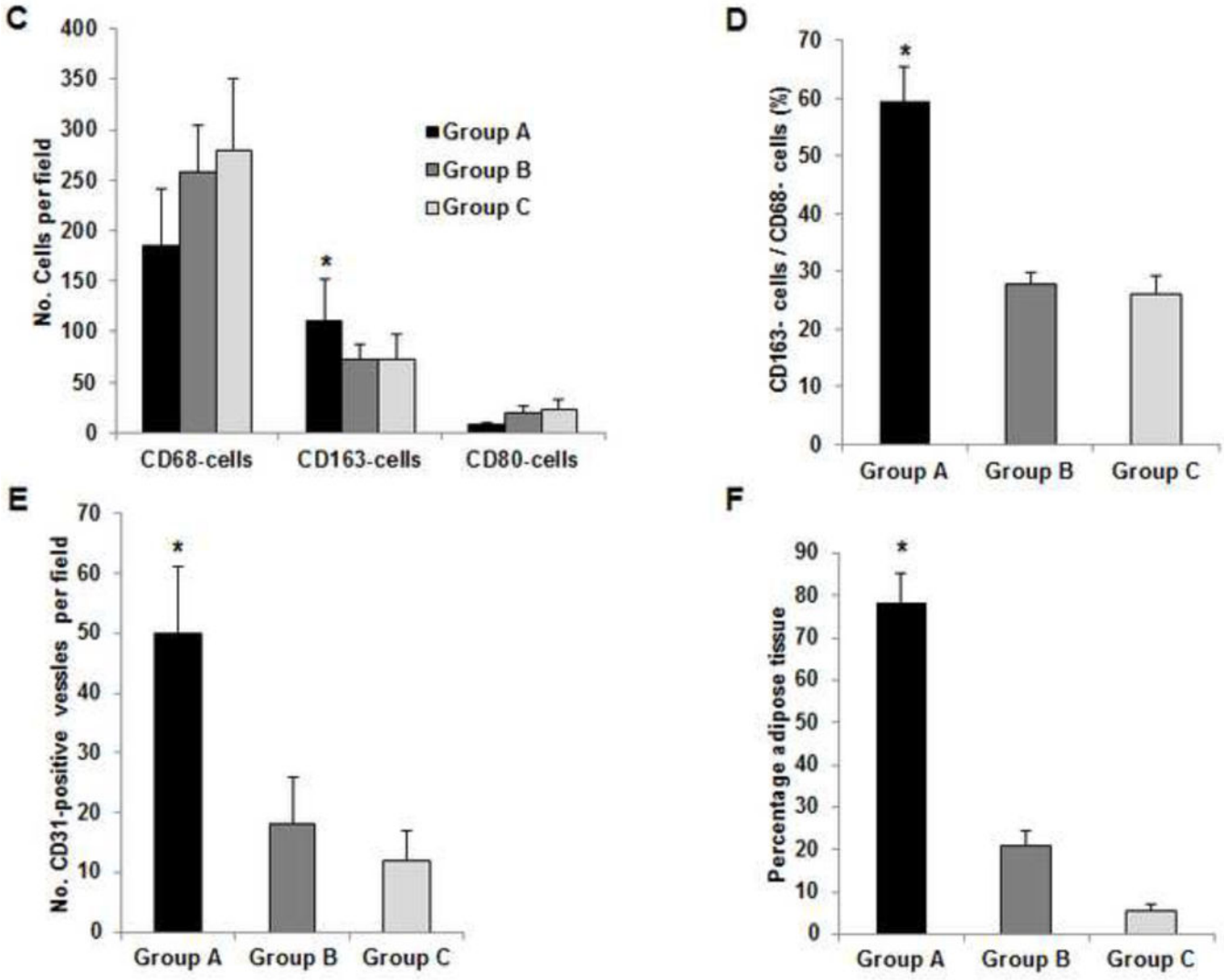

Fig. 8. IHC analysis of explants in groups B and C at 3 months

(A) Explanted samples of group B and C were relatively hard with lots of undegraded dermis. Masson trichrome staining showed fibrotic remodeling in most areas of the explants. There were only a few vessels located in the vascular pedicle area (third images). The much lower vascularization resulted in less adipose regeneration in the tissues of both groups. *: adipose tissue. (B) Compared to CD80-positive M1 cells (blue arrow), relatively high numbers of CD163-positive M2 cells (red arrow) were distributed in the tissues. Numerous CD68-positive macrophages (black arrow) infiltrated the tissues in both groups. (C) At 3 months, there were significantly more CD163-positive macrophages in the tissue of group A than in the tissues of groups B or C. *: $P<0.05$ as compared to groups B and C. (D) The ratio of CD163-positive cells to CD68-positive cells in group A was significantly higher than those in groups B and C at 3 months. *: $P<0.05$ as compared to groups B and C. (E) There were significantly more CD31-positive vessels in the tissue of group A than in the tissues of groups B and C at 3 months. *: $P<0.05$ as compared to groups B and C. (F) At 3 months, the

area of adipose tissue in group A was significantly greater than that in groups B and C. *: $P<0.05$ as compared to groups B and C.

Table 1

Morphology of hASCs on DSAF scaffold and 2-dimensional (2D) glass slides on days 1 and 7 of culture.

	DSAF Scaffold			2D Glass Slides		
	Area (μm^2)	**Perimeter (μm)**	**Circularity**	**Area (μm^2)**	**Perimeter (μm)**	**Circularity**
Day 1	$1.8\times10^2\pm0.93\times10^2$ (n=20)	$0.6\times10^2\pm0.18\times10^2$ (n=20)	0.531±0.142 (n=20)	$1.35\times10^3\pm0.83\times10^3$ (n=18)	$3.3\times10^2\pm0.11\times10^2$ (n=18)	0.13±0.044 (n=18)
Day 7	$1.2\times10^2\pm0.33\times10^2$ (n=20)	$0.49\times10^2\pm0.082\times10^2$ (n=20)	0.585±0.122 (n=20)	$3.3\times10^3\pm1.4\times10^3$ (n=19)	$4.1\times10^2\pm0.36\times10^2$ (n=19)	0.22±0.075 (n=19)

Note: Values are means ± standard deviations. Differences in all parameters between the DSAF scaffold and 2D glass slides at the same time points were significant (P<0.05).